Influence of pH on Ca^{2+} current and its control of electrical and Ca^{2+} signaling in ventricular myocytes

Noriko Saegusa,[1] Emma Moorhouse,[2] Richard D. Vaughan-Jones,[2] and Kenneth W. Spitzer[1]

[1]Department of Physiology, Nora Eccles Harrison Cardiovascular Research and Training Institute, University of Utah, Salt Lake City, UT 84112

[2]Department of Physiology, Anatomy and Genetics, Burdon Sanderson Cardiac Science Centre, Oxford University, Oxford OX1 3PT, England, UK

Modulation of L-type Ca^{2+} current ($I_{Ca,L}$) by H^+ ions in cardiac myocytes is controversial, with widely discrepant responses reported. The pH sensitivity of $I_{Ca,L}$ was investigated (whole cell voltage clamp) while measuring intracellular Ca^{2+} (Ca^{2+}_i) or pH_i (epifluorescence microscopy) in rabbit and guinea pig ventricular myocytes. Selectively reducing extracellular or intracellular pH (pH_o 6.5 and pH_i 6.7) had opposite effects on $I_{Ca,L}$ gating, shifting the steady-state activation and inactivation curves to the right and left, respectively, along the voltage axis. At low pH_o, this decreased $I_{Ca,L}$, whereas at low pH_i, it increased $I_{Ca,L}$ at clamp potentials negative to 0 mV, although the current decreased at more positive potentials. When Ca^{2+}_i was buffered with BAPTA, the stimulatory effect of low pH_i was even more marked, with essentially no inhibition. We conclude that extracellular H^+ ions inhibit whereas intracellular H^+ ions can stimulate $I_{Ca,L}$. Low pH_i and pH_o effects on $I_{Ca,L}$ were additive, tending to cancel when appropriately combined. They persisted after inhibition of calmodulin kinase II (with KN-93). Effects are consistent with H^+ ion screening of fixed negative charge at the sarcolemma, with additional channel block by H^+_o and Ca^{2+}_i. Action potential duration (APD) was also strongly H^+ sensitive, being shortened by low pH_o, but lengthened by low pH_i, caused mainly by H^+-induced changes in late Ca^{2+} entry through the L-type Ca^{2+} channel. Kinetic analyses of pH-sensitive channel gating, when combined with whole cell modeling, successfully predicted the APD changes, plus many of the accompanying changes in Ca^{2+} signaling. We conclude that the pH_i-versus-pH_o control of $I_{Ca,L}$ will exert a major influence on electrical and Ca^{2+}-dependent signaling during acid–base disturbances in the heart.

The Journal of General Physiology

INTRODUCTION

The flow of L-type Ca^{2+} current ($I_{Ca,L}$) into ventricular myocytes links excitation to myocardial contraction. The current, conducted through $Ca_v1.2$ protein channels, is activated during an action potential (AP) and induces Ca^{2+} release from the SR (Bers, 2001; Bodi et al., 2005; Dolphin, 2006). The resulting cytoplasmic Ca^{2+} transient (CaT) triggers myofilament interaction and hence cellular contraction. $I_{Ca,L}$ is also an integral component of the electrical signal itself, contributing to the plateau phase of the ventricular AP. The current is modulated by neurotransmitters, hormones, and the intracellular levels of Ca^{2+}. In addition, it is modulated by H^+ ions, with most reports indicating inhibition at low intracellular pH (pH_i) or extracellular pH (pH_o) (Kohlhardt et al., 1976; Kurachi, 1982; Yatani and Goto, 1983; Irisawa and Sato, 1986; Kaibara and Kameyama, 1988; Krafte and Kass, 1988; F. Chen et al., 1996; Cheng et al., 2009). H^+ ions are common end-products of metabolism, and their enhanced production can decrease myocardial pH during an increased workload (Bountra et al., 1988; Elliott et al., 1994) or during clinical disorders like myocardial ischemia (Garlick et al., 1979; Yan and Kléber, 1992). Excitation–contraction coupling in myocytes is therefore functionally linked to cellular pH regulation, a process accomplished by acid-transporting proteins in the sarcolemma, such as Na/H exchange (NHE), Na-HCO_3 cotransport, and the monocarboxylic acid transporter (Vaughan-Jones et al., 2009).

Although there is considerable literature on the influence of pH on $I_{Ca,L}$ in the heart, the reported effect has varied widely, from virtually nothing (Komukai et al., 2001; Salameh et al., 2002) to profound inhibition during acidosis (Krafte and Kass, 1988). In cases where pH_i in ventricular myocytes has been manipulated experimentally, apparent differences in the effect may have stemmed from a lack of precise measurement of pH_i. In addition, some protocols altered both pH_i and pH_o, and the possibility of potentiating or conflicting effects of the two pH domains on $I_{Ca,L}$ has not been explored so

Correspondence to Kenneth W. Spitzer: spitzer@cvrti.utah.edu

Abbreviations used in this paper: AP, action potential; APD, AP duration; Ca^{2+}_i, intracellular Ca^{2+}; CaMK, calmodulin kinase; CaT, Ca^{2+} transient; CDI, calcium-dependent inactivation; CL, cycle length; $I_{Ca,L}$, L-type Ca^{2+} current; I_{NCX}, NaCa exchange current; I_{ns}, nonspecific current; NHE, Na/H exchange; pH_i, intracellular pH; pH_o, extracellular pH; SERCA, SR Ca^{2+}-ATPare; VDI, voltage-dependent inactivation.

The Rockefeller University Press $30.00
J. Gen. Physiol. Vol. 138 No. 5 537–559
www.jgp.org/cgi/doi/10.1085/jgp.201110658

far (Komukai et al., 2002). In addition, a fall of pH_i or pH_o leads to complex and often dynamic changes of intracellular Ca^{2+} (Ca^{2+}_i), which are likely to feed back and alter $I_{Ca,L}$. For example, a fall of pH_i raises diastolic Ca^{2+} in ventricular myocytes (Gambassi et al., 1993), and a rise of Ca^{2+}_i can promote inactivation of $I_{Ca,L}$ (You et al., 1997). Finally, calmodulin kinase (CaMK)II activity is reported to protect $I_{Ca,L}$ from the acute inhibitory effects of acidosis, possibly by enhancing phosphorylation of the $Ca_v1.2$ protein (Komukai et al., 2001).

In this work, we quantify the acute control of $I_{Ca,L}$ by increased H^+ ion concentration in rabbit and guinea pig ventricular myocytes. To do this, we manipulate pH while measuring the kinetic and gating properties of $I_{Ca,L}$ using whole cell voltage clamp, often in conjunction with fluorescence measurements of Ca^{2+}_i or pH_i. We specifically explore the role of pH_i and pH_o, testing whether the two pH domains exert separate effects on $I_{Ca,L}$. We attempt to dissect out secondary effects of H^+ ions, caused by their influence on Ca^{2+}_i, and we examine if the acute influence of pH is significantly modulated by CaMKII activity. To assess the physiological consequences of a pH-induced change in $I_{Ca,L}$, we document effects on the ventricular AP and Ca^{2+} signaling. Using mathematical modeling, we are able to elucidate how H^+ modulation of $I_{Ca,L}$ can produce novel and often counterintuitive effects on ventricular myocyte function. A major insight is that pH_i and pH_o can exert opposite effects on $I_{Ca,L}$ gating and net Ca^{2+} entry through the channel, with consequent effects on the AP and Ca^{2+} handling.

MATERIALS AND METHODS

Myocyte isolation

Experiments were performed on adult ventricular myocytes isolated from rabbit and guinea pig by enzymatic digestion as described previously (Yamamoto et al., 2005). All procedures involving animals were approved by the Animal Care and Use Committee of the University of Utah and complied with the National Institutes of Health Guide for the Care and Use of Laboratory Animals 1996 and the UK Animals (Scientific Procedures) Act 1986 guidelines.

Cell chamber, bathing solutions, and drugs

Isolated cells were superfused at 4 ml/min (37 ± 0.3°C), with solution exchange within the experimental chamber occurring in ~5 s. The glass base of the chamber was coated with laminin (Collaborative Research) to improve cell adhesion.

Three types of acidosis were applied to myocytes: extracellular acidosis (pH_o 6.5, with a normal pH_i of 7.1), intracellular acidosis (pH_i 6.7, with a normal pH_o of 7.4), and combined acidosis (pH_i 6.7 and pH_o 6.5). As described below, all bathing solutions contained 30 µM cariporide to block NHE, and, except for the respiratory acidosis experiments (Fig. S2), all were buffered with HEPES with no added CO_2 or HCO_3^-.

Because it was important to maintain a constant extracellular free Ca^{2+} activity during these solution changes, this parameter was measured at 37°C with an electrolyte analyzer (Nova 8; Nova Biomedical). The normal control solution for extracellular acidosis and intracellular acidosis contained (in mM): 126.0 NaCl, 11.0 dextrose, 4.4 KCl, 1.0 $MgCl_2$, 1.08 $CaCl_2$, and 24.0 HEPES, titrated to pH 7.4 with 1 M NaOH. This solution also served as the control solution in experiments involving superfusion with 30% CO_2. The solution used to create extracellular acidosis had the same composition, except its pH was titrated to 6.5 with NaOH. Its Ca^{2+} activity was the same as the control solution.

The solution used to induce intracellular acidosis with pH_o held at 7.4 was prepared by equimolar replacement of 80 mM sodium acetate (NaAc) in the control solution for NaCl. Decreasing pH_i by application of extracellular acetate is a widely used technique and results from rapid influx of uncharged protonated acetate, which then releases protons intracellularly (Thomas, 1984) while the pH of the superfusate remains constant at 7.4. However, a problem with using acetate (or other salts of weak acids, like propionate or butyrate) is the binding of Ca^{2+} to the free anion (Kenyon and Gibbons, 1979; Hacht, 2008). Thus, it was necessary to increase $CaCl_2$ in the 80-mM acetate solution from 1.08 to 1.37 mM to keep Ca^{2+} activity the same as in control solutions. Note that in part because of intrinsic Ca^{2+} buffering within cells, intracellular acetate does not significantly reduce Ca^{2+}_i.

The control solution used for combined acidosis experiments contained (in mM): 96.0 NaCl, 30.0 NaAc, 11.0 dextrose, 4.4 KCl, 1.0 $MgCl_2$, 1.29 $CaCl_2$, and 24.0 HEPES, titrated to pH 7.4 with 1 M NaOH. Myocytes were first bathed in this solution without cariporide for 20 min to allow pH_i to recover from the intracellular acid load caused by influx of protonated acetate. After this equilibration period, the same solution, with 30 µM cariporide, was applied for at least 2 min, and then control measurements of $I_{Ca,L}$, APs, and CaTs were obtained. These parameters were not significantly different from those in the normal control solution without NaAc. Combined acidosis was then induced by switching from the control solution to one with the same composition titrated to pH 6.5 with NaOH. During voltage-clamp experiments, potassium chloride was replaced with 4.4 mM CsCl in the control and acid-inducing solutions for each type of acidosis (extracellular, intracellular, and combined).

In some experiments, we also tested the effect of acidosis on $I_{Ca,L}$ with Na^+ as the charge carrier (nonspecific current [I_{ns}]). We chose Na^+ because it avoids the ion-dependent inactivation seen with Ba^{2+} as the charge carrier (Ferreira et al., 1997). The bathing solutions for control, extracellular, and intracellular acidosis (pH_o 7.4) had the same compositions as those described above, except they contained 0.5 mM EGTA and no added Ca^{2+}. Na^+ and Mg^{2+} concentrations were held at 138.9 and 1.0 mM, respectively, and CsCl replaced KCl. Although Mg^{2+} decreases Na^+ influx via L-type Ca^{2+} channels (Matsuda, 1986), its presence in the extracellular solution attenuates the leftward shift in the I-V curve induced by removing all divalent cations.

The control Cl^--free bathing solution used in $I_{Ca,L}$ voltage-clamp experiments contained (in mM): 126 sodium glucuronate, 11 dextrose, 1.0 $MgSO_4$, 4.0 calcium gluconate, and 24.0 HEPES, titrated to pH 7.4 with 1 M NaOH. The high concentration of calcium gluconate was required to keep Ca^{2+} activity the same as that in normal Cl^- control solution. The Cl^--free solution (pH_o 7.4) used to create intracellular acidosis had the same composition as the control Cl^--free solution, except for equimolar replacement of 80 mM NaAc for sodium glucuronate and 3.61 mM for calcium gluconate.

In other experiments, a combined extracellular/intracellular (respiratory) acidosis was induced by switching from the normal HEPES-buffered control solution (no acetate, pH_o 7.4) to one containing (in mM): 126 NaCl, 11 dextrose, 4.4 KCl, 1.0 $MgCl_2$, 1.08 $CaCl_2$, and 18.5 $NaHCO_3$. It was continuously gassed with 30.0% CO_2–70.0% O_2 to give a pH of 6.6. Its calcium activity was the same as the normal control solution.

Except for the initial equilibration period in the control solution for combined acidosis, all bathing solutions (control and acid-inducing) contained 30 μM cariporide (Sanofi-Aventis) to block selectively NHE. Na-HCO_3^- cotransport was inhibited in the respiratory acidosis experiments by including 10 μM S-0859 (Sanofi-Aventis; Ch'en et al., 2008). 1 μM KN-93 (EMD) was included in bathing solutions to inhibit CaMKII. $I_{Ca,L}$ was blocked by including 10 μM nifedipine (Sigma-Aldrich) and 300 μM $CdCl_2$ in the bathing solutions.

Pipette filling solutions

The normal filling solution used for $I_{Ca,L}$ voltage-clamp experiments was similar to that described by Wu et al. (1999) and contained (in mM): 120.0 CsCl, 5.0 NaCl, 10.0 tetraethylammonium chloride (TEA-Cl), 5.0 MgATP, 5.0 phosphocreatine, 1.0 NaGTP, and 10.0 HEPES, titrated to pH 7.2 with 1 M CsOH. A solution containing 5 mM BAPTA (free acid) with the same composition and pH was used in several voltage-clamp experiments to prevent CaTs and block the rise in diastolic Ca^{2+} induced by intracellular and combined acidosis. BAPTA is preferable to EGTA because of its faster Ca^{2+}-binding kinetics and lower pH sensitivity (Tsien, 1980). This concentration of BAPTA also avoids the stimulation of $I_{Ca,L}$ by disinhibiting calcium-sensitive adenylyl cyclase (You et al., 1997).

The filling solution used in the Cl^--free voltage-clamp experiments of $I_{Ca,L}$ contained (in mM): 120.0 cesium aspartate, 5.0 sodium glucuronate, 10.0 TEA-Cl, 5.0 MgATP, 5.0 phosphocreatine, 1.0 NaGTP, and 10.0 HEPES, titrated to pH 7.2 with 1 M CsOH. 10 mM Cl^- was included to maintain a stable junction with the AgAgCl pellet in the pipette. Corrections were made for liquid junction potentials.

The normal filling solution used for recording APs contained (in mM): 110.0 KCl, 5.0 NaCl, 5.0 MgATP, 5.0 phosphocreatine, 1.0 NaGTP, and 10.0 HEPES, titrated to pH 7.2 with 1 M KOH. In some experiments, this solution also contained 5.0 mM BAPTA to buffer intracellular calcium and block CaTs. The pipette solution used to record APs in chloride-free bathing solution contained (in mM): 10.0 KCl, 110.0 K gluconate, 5.0 Na glucuronate, 5.0 MgATP, 5.0 phosphocreatine, 1.0 NaGTP, and 10.0 HEPES, titrated to pH 7.2 with 1 M KOH. Corrections were made for liquid junction potentials.

Electrophysiological techniques

All voltage-clamp and AP measurements were made with whole cell ruptured patch pipettes. Pipettes (8250 glass; Corning) had resistances of 1–2 MΩ when filled. APs were recorded with an amplifier system (Axoclamp-2A; Axon Instruments) in bridge mode, and voltage clamping (step clamps and AP clamps) was achieved with an Axopatch 200 B clamp system (Axon Instruments). APs recorded in bridge mode were triggered with brief rectangular pulses of depolarizing intracellular current. AP duration (APD) was measured at 90% repolarization (APD_{90}). 30 μM cariporide had no effect on the time course or duration of the AP of either guinea pig or rabbit ventricular myocytes (n = 6 and 5 cells, respectively; not depicted).

Membrane potential (V_m) and $I_{Ca,L}$ were filtered at 5 kHz, digitized at 50 kHz with a 16-bit A/D converter (Digidata 1322A; Molecular Devices) and analyzed using PCLAMP 8 software (Molecular Devices). The reference electrode was a flowing 3-M KCl bridge. Compensation for series resistance (75–80%) and capacitance was performed electronically. $I_{Ca,L}$ was normalized for cell capacitance (pA/pF).

Peak I-V relationships for $I_{Ca,L}$. These were determined by applying test pulses from −40 to +60 mV (400-msec duration) at a cycle length (CL) of 5 s. Each test pulse was preceded by a prepulse from a holding potential of −80 to −40 mV (duration of 200 msec) to inactivate sodium current. By initiating clamp steps from −40 mV, contamination of the $I_{Ca,L}$ signal by T-type calcium current in guinea pig myocytes was also avoided (Sipido, et al., 1998). Rabbit ventricular myocytes are reported to have no T-type calcium current (Yuan et al., 1996). This clamp protocol was applied first in the control solution and then after 2 min in the acidic test solution. Each cell was exposed only once to an acidic test solution. The same clamp protocol was used to measure I_{ns}, except the clamp durations were 1 s and the most positive step was to +40 mV. All $I_{Ca,L}$ measurements were performed in the presence of 30 μM cariporide to block NHE. In separate experiments, we found that 30 μM cariporide did not affect $I_{Ca,L}$ in either rabbit (n = 9) or guinea pig ventricular myocytes (n = 4). In contrast, another commonly used NHE inhibitor, amiloride (1 mM; pH_o 7.4), reduced guinea pig $I_{Ca,L}$ by 49 ± 17% after a 2-min exposure (n = 4), in accord with previous observations (Cheng et al., 2004). All $I_{Ca,L}$ and I_{ns} signals were background corrected by applying the same clamp and solution protocol to several separate cells with $I_{Ca,L}$ blocked using 10 μM nifedipine plus 300 μM $CdCl_2$.

Steady-state voltage dependence of $I_{Ca,L}$ activation (d_∞). This was determined using results obtained from the I-V curve-clamp protocol. $I_{Ca,L}$ conductance (G) at each voltage step was calculated as $G = I_{Ca,L}/(V_m - V_{rev})$, where V_m is the clamp potential and V_{rev} is the apparent reversal potential, extrapolated from the rising portion of the I-V curve. The results were plotted as G/G_{max} as a function of V_m and best fit with a Boltzmann function, $G/G_{max} = 1/[1 + \exp\{(V_m - V_{1/2})/k\}]$, where $V_{1/2}$ and k are the half-maximal activation potential and the slope (mV) of the curve, respectively.

Steady-state voltage dependence of $I_{Ca,L}$ inactivation (f_∞). This was determined using a double pulse protocol. Conditioning clamp pulses ranging from −40 to 0 mV (1-s duration) were initiated from a holding potential of −80 mV at a CL of 5 s. At the end of each conditioning pulse, V_m was clamped to −40 mV for 10 msec before applying the test pulse to +10 mV (near peak of the I-V curves). Peak currents elicited by the test pulses were normalized as $I_{Ca,L}/I_{Ca,Lmax}$ and plotted as a function of conditioning V_m. The curves were fit with a Boltzmann function, $I_{Ca,L}/I_{Ca,Lmax} = A + (1 - A)/[1 + \exp\{(V_m - V_{1/2})/k\}]$, where A is the value of f_∞ at 0 mV, V_m is the conditioning voltage, and $V_{1/2}$ and k are the half-maximal inactivation potential and the slope (mV) of the curve, respectively.

Quantifying the time course of $I_{Ca,L}$ inactivation. The clamp protocol was the same as that used to generate I-V curves. The time course of inactivation of $I_{Ca,L}$ was fit with a double exponential according to:

$$I = A_f e^{-t/\tau_f} + A_s e^{-t/\tau_s} + C, \quad (1)$$

where I is the current (pA/pF) at time t (msec); A_f (pA/pF) and A_s (pA/pF), respectively, are the amplitudes of fast and slow components; τ_f and τ_s, respectively, are the fast and slow inactivation time constants (msec); and C is the current remaining at the end of the clamp step (pA/pF).

AP voltage clamp (AP clamp). Experiments were performed to assess the effects of the three acidosis maneuvers on $I_{Ca,L}$ under more physiological conditions. The bathing and pipette solutions used for these experiments were the same as those used to generate the I-V curves for each type of acidosis. AP templates were obtained from representative records obtained during current-clamp experiments. Clamp pulses were applied at a CL of 5 or 2 s from a holding potential of −40 mV (50-msec duration) to inactivate sodium current. Each AP clamp was preceded by a prepulse from −85 to −40 mV, either as a step or a 300-msec duration ramp. First, a train of 10 conditioning clamps was applied in the

control solution using the control AP template. They were then repeated after 2 min in the test solution using the appropriate test AP template. The entire protocol was then repeated in the presence of 10 µM nifedipine plus 300 µM $CdCl_2$ to block $I_{Ca,L}$. The difference current was used to determine $I_{Ca,L}$ flowing during the AP. Net calcium influx (pC/pF) via $I_{Ca,L}$ was measured by integrating $I_{Ca,L}$ over the time course of the AP clamp.

Contamination of nifedipine/cadmium-sensitive current by NaCa exchange current (I_{NCX}). To activate $I_{Ca,L}$ accompanied by normal CaTs, we did not buffer intracellular calcium in many of the voltage-clamp experiments using both conventional depolarizing rectangular-shaped pulses and AP clamps. In this setting, inward I_{NCX} (3 Na^+ in/1 Ca^{2+} out) will also be activated by any rise in cytosolic Ca^{2+}. The application of nifedipine/cadmium solution will not only directly block $I_{Ca,L}$, by preventing the CaT, it will also indirectly inhibit the $Ca^{2+}{}_i$ activation of inward I_{NCX}. Thus, we cannot rule out possible contamination of the measured nifedipine/cadmium-sensitive current by Ca^{2+}-activated changes of I_{NCX}. However, we have previously shown that peak $I_{Ca,L}$ is much greater than peak inward I_{NCX} measured in the same cell (Bridge et al., 1990). In addition, computer simulations of $I_{Ca,L}$ and I_{NCX} during APs or conventional voltage clamp (rabbit ventricular myocyte models; Shannon et al., 2004; Mahajan et al., 2008) demonstrate that peak inward I_{NCX} is small compared with peak $I_{Ca,L}$ and occurs significantly after the latter (see also Fig.11 of this work). Thus, it seems unlikely that acid-induced changes in I_{NCX} will significantly contaminate our I-V curves of peak nifedipine/cadmium-sensitive current. To help address this issue experimentally, we performed voltage-clamp experiments (either conventional rectangular-shaped pulses or AP clamps) with BAPTA in the pipette to prevent the CaT and thus inhibit changes of Ca^{2+}-activated I_{NCX} (Bridge et al., 1990). The results indicate that the nifedipine/cadmium-sensitive current we measured was predominantly $I_{Ca,L}$.

Measurement of pH_i and Ca^{2+}

pH_i was measured in single resting myocytes with carboxyseminaphthorhodafluor-1 as described previously in detail (Buckler and Vaughan-Jones, 1990; Spitzer and Bridge, 1992). $Ca^{2+}{}_i$ was monitored with epifluorescence in single myocytes with the fluorescent indicator, fluo-4. Cells were incubated in the normal control solution containing 10 µM fluo 4-AM (Invitrogen) and 0.3 mM probenicid at 30°C for 20 min. 0.3 mM probenicid was included in the bathing solutions to help retard fluo-4 loss from the cells. Fluorescence emission (535 nm, bandpass filter) was collected with a photomultiplier tube via the 40× objective during continuous excitation at 485 nm. CaTs were initiated with either field stimulation or with current injection through the attached suction pipette.

Estimating SR Ca^{2+} content. This was quantified from the integrated inward I_{NCX}, triggered by rapid application of 20 mM caffeine as described previously (Choi et al., 2000). No corrections were made for Ca^{2+} efflux via the sarcolemmal Ca^{2+} pump. The high caffeine concentration helped to ensure complete SR Ca^{2+} release. The caffeine pulse was preceded by at least 15 conditioning AP-clamp pulses (CL = 2 s), with a holding potential between pulses of −85 mV. The control and acidic AP templates for the conditioning clamp pulses were the same as those used for $I_{Ca,L}$ measurements (Fig. 8).

Statistics

Summarized results are expressed as mean ± SEM. A paired Student's *t* test was used to test significance between results obtained with each cell serving as its own control. An unpaired *t* test was used to test significance between results obtained on different cells. $P < 0.05$ was considered significant.

Online supplemental material

Fig. S1 illustrates the lack of effect of pipette attachment on pH_i in a rabbit ventricular myocyte. Fig. S2 illustrates the effects of respiratory acidosis on pH_i, AP configuration, and CaTs in rabbit ventricular myocytes. Fig. S3 shows the effects of acidosis on $I_{Ca,L}$ I-V curves in guinea pig ventricular myocytes. It also includes the effect of intracellular acidosis on rabbit I-V curves measured in chloride-free solution. Fig. S4 shows the effect of BAPTA dialysis (5 mM) on CaTs and the rise in diastolic calcium elicited by intracellular acidosis in a rabbit ventricular myocyte. Fig. S5 summarizes rabbit $I_{Ca,L}$ inactivation kinetics during BAPTA dialysis. Fig. S6 summarizes the effects of extracellular and intracellular acidosis on rabbit I_{ns}. Fig. S7 summarizes the effects of the three types of acidosis on rabbit $I_{Ca,L}$ during AP voltage clamps with BAPTA dialysis. Table S1 summarizes the effects of acidosis in rabbit $I_{Ca,L}$ activation parameters with and without BAPTA dialysis. Table S2 summarizes the effects of acidosis on rabbit $I_{Ca,L}$ steady-state inactivation parameters with and without BAPTA dialysis. Table S3 summarizes the effects of acidosis on the voltage dependence of rabbit $I_{Ca,L}$ inactivation kinetics without BAPTA dialysis. Table S4 summarizes the effects of BAPTA dialysis on the voltage dependence of rabbit $I_{Ca,L}$ inactivation kinetics under control conditions (no acidosis). The online supplemental material is available at http://www.jgp.org/cgi/content/full/jgp.201110658/DC1.

RESULTS

Effect of acidosis on the AP

The left-hand panels in Fig. 1 illustrate, in rabbit ventricular myocytes, the experimental protocols used to reduce pH_o, pH_i, or both. Bicarbonate transporter activity was minimized by superfusing CO_2/HCO_3^--free solution, and NHE activity was blocked with 30 µM cariporide. As shown in Fig. 1 A (i), 2 min of extracellular acidosis (pH_o 6.5) caused virtually no change of pH_i (reduced by ∼0.05 U to pH_i 7.12 ± 0.06; $n = 7$). In contrast, 2 min of acetate superfusion (80 mM) at a constant pH_o of 7.4 acidified pH_i by ∼0.5 U to pH_i 6.75 ± 0.04 ($n = 17$; Fig. 1 B, i). Similar results were observed in guinea pig ventricular myocytes ($n = 9$; not depicted). After 2 min of the combined acidosis protocol (pH_o 6.5 plus 30 mM acetate), pH_i also acidified by ∼0.5 U to pH_i 6.67 ± 0.08 ($n = 7$; Fig. 1 C, i). The 2-min protocol for the three types of acidosis was used in all subsequent work.

Selectively reducing pH_o shortened the AP in rabbit myocytes and depressed the early plateau phase (Fig. 1 A, ii). In contrast, selectively reducing pH_i lengthened the AP, slowed phase 1 repolarization, and elevated the plateau (Fig. 2 B, ii). The latter two effects were a result, in part, of suppression of transient outward K current, I_{to}, by low pH (Saegusa, N., V. Garg, and K.W. Spitzer. 2011. Transient outward current responds differently to external and internal protons in ventricular myocytes. Heart Rhythm Society Meeting. Abstr. S252). The AP response to a combined reduction of pH_i and pH_o was very similar to that of low pH_i (Fig. 1 C, ii). We conclude that a fall of pH exerts opposite effects on the AP, depending on whether the acidosis occurs in the extracellular or

intracellular domain. Intracellular acidosis lengthens while extracellular acidosis shortens APD.

A comparable AP prolongation during low pH_i was observed when experiments were performed in the absence of Cl^-_o (Cl^- replaced by gluconate), indicating that it was not caused by changes in Cl^- current. Furthermore, pH_i itself was unaffected by attachment of the suction pipette used to record the AP (Fig. S1).

Effect of acidosis on electrically evoked CaTs

The effects of acidosis on CaTs in field-stimulated rabbit myocytes (0.5 Hz) are illustrated in Fig. 2. All three types of acidosis (low pH_o, low pH_i, and low pH_o and pH_i) elicited an initial drop in systolic Ca^{2+}, followed by a secondary recovery (Fig. 2, A and B, a) that was nearly complete by 2 min. This recovery occurred despite the sustained fall of pH_i during the intracellular and

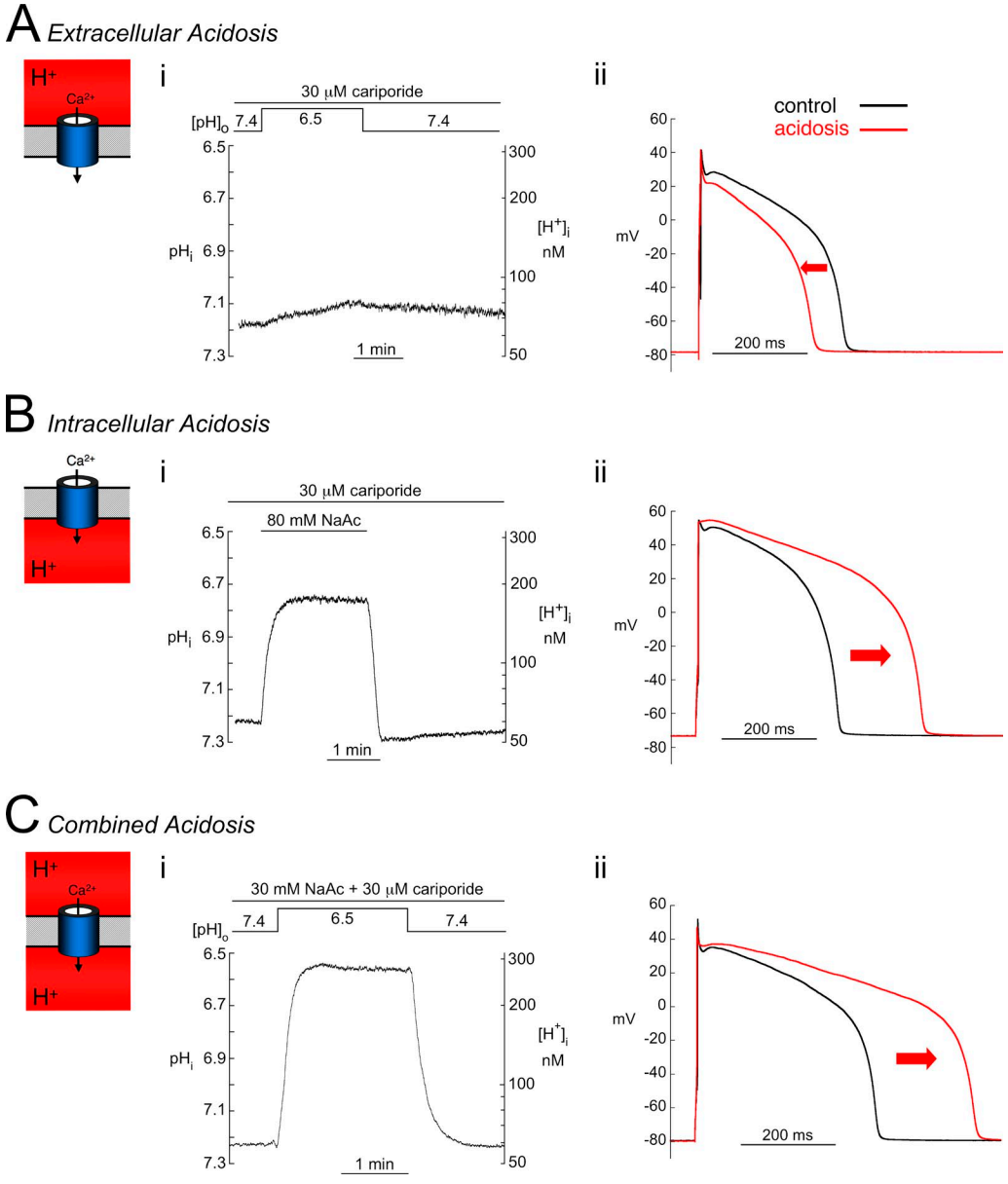

Figure 1. Acidosis and electrical signaling. Changes in pH_i, $[H^+]_i$, and AP induced by extracellular, intracellular, and combined acidosis (see cartoon insets) in rabbit myocytes (A; i). A reduction in pH_o from 7.4 to 6.5 for 2 min elicited only a small drop in pH_i. (ii) Extracellular acidosis (2 min; red) shortened APD and depressed the plateau (APD_{90}, control = 336 ± 33 msec and low pH_o = 279 ± 31 msec; n = 9; P < 0.01, paired). (B; i) In contrast, exposure to 80.0 mM acetate, pH_o 7.4, induced a rapid sustained fall in pH_i. (ii) Intracellular acidosis (2 min; red) prolonged APD, slowed phase 1 repolarization, and elevated the plateau (APD_{90}, control = 324 ± 29 msec and low pH_i = 491 ± 31 msec; n = 15; P < 0.01, paired). (C; i) Combined acidosis (2 min; red) involved reducing pH_o from 7.4 to 6.5 in the presence of 30 mM acetate. pH_i fell by approximately the same extent as with intracellular acidosis alone (B). (ii) Combined acidosis elicited changes in the AP that were similar to those during intracellular acidosis (APD_{90}, control = 343 ± 24 and combined acidosis = 481 ± 30 msec; n = 6; P < 0.01, paired). The control values of pH_i for each type of acidosis were very similar: extracellular acidosis, 7.18 ± 0.05 (n = 7); intracellular acidosis, 7.22 ± 0.02 (n = 17); and combined acidosis, 7.16 ± 0.04 (n = 7).

combined acidosis protocols (Fig. 1). Accompanying the secondary recovery of systolic calcium was a rise in diastolic Ca^{2+} ($[Ca^{2+}]_{dia}$; Fig. 2 B, b). The smallest rise occurred during extracellular acidosis and was difficult to detect in some cells (e.g., Fig. 2 A, left). As a result of the systolic and diastolic changes, CaT amplitude was reduced by 20–30% in all three types of acid challenge and displayed only a small recovery during the 2-min period (Fig. 2 B, c). The maximum rate of rise in the time course of the CaT (CaT derivative) showed a sustained decrease that was largest during intracellular and combined acidosis (Fig. 2 B, d). In addition, CaT duration was prolonged by intracellular and combined acidosis but shortened slightly by extracellular acidosis (Fig. 2 B, e). The changes in CaT duration were fully reversible and correspond qualitatively to the changes in APD (Fig. 1). Similar effects of acidosis on Ca^{2+} signaling were observed in experiments on myocytes paced at 2.0 instead of 0.5 Hz ($n = 9$; not depicted).

To exclude the possibility that acetate per se may have directly affected the AP and CaT, we superfused a CO_2/HCO_3^--buffered solution (30.0% CO_2, pH_o 6.6, and 18.5 mM HCO_3^-) instead of acetate to induce a combined (respiratory) acidosis (Fig. S2). The decreases of pH_i and pH_o, and the subsequent prolongation of AP and CaT, were very similar to those seen with acetate-containing solution (compare Fig. 1 C with Fig. 2 A, right). Thus, acetate per se does not appear to exert direct effects, with results being attributable to the changes of pH_i and pH_o.

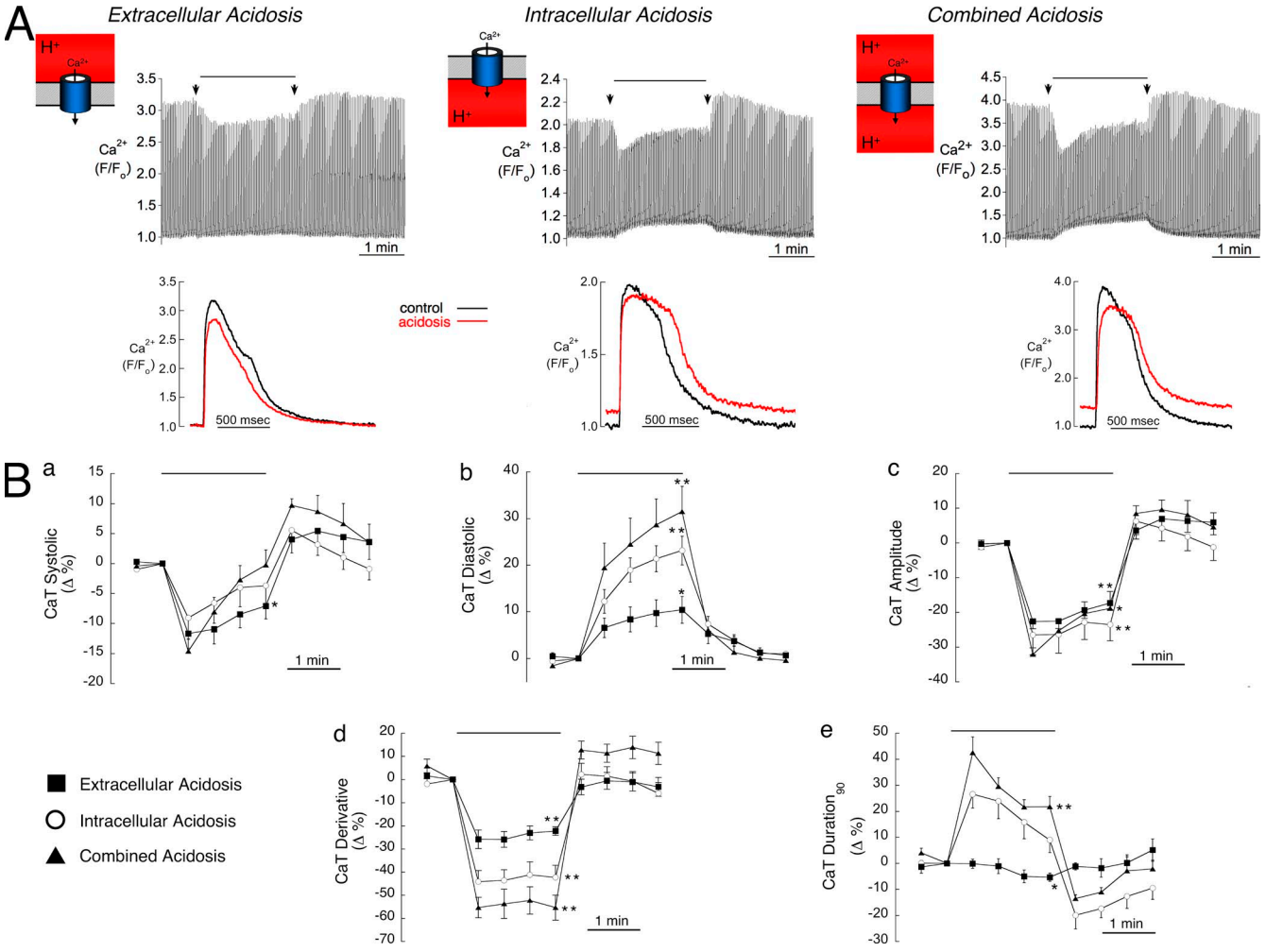

Figure 2. Acidosis and Ca^{2+} signaling. Time course of changes in CaTs during extracellular, intracellular, and combined acidosis. Myocytes (rabbit) were field stimulated at CL = 2 s. (A) Representative examples from three cells showing the effects of a 2-min application of the acidifying solutions. Below each panel are the CaTs recorded during control and after 2 min of acidosis (red), indicated by arrows. (B) Summarized CaT parameters for extracellular ($n = 7$), intracellular ($n = 12$), and combined acidosis ($n = 6$). Results are expressed as percent change relative to control immediately before applying the acidifying solutions. (a) CaT systolic, systolic value of the CaT; (b) CaT diastolic, diastolic value of the CaT; (c) CaT amplitude, amplitude of the CaT; (d) CaT derivative, rate of rise of the CaT (arbitrary units); (e) CaT $duration_{90}$, duration of the CaT at 90% recovery. **, $P < 0.01$; *, $P < 0.05$, paired; control compared with 2 min of acidosis.

Effect of acidosis on SR Ca^{2+} content

As well as altering cytoplasmic Ca^{2+}, acidosis affects the SR Ca^{2+} load by altering Ca^{2+} release and reuptake processes (Hulme and Orchard, 1998). Under normal conditions, for a given magnitude of $I_{Ca,L}$, the amplitude of CaT is steeply dependent on SR load (Shannon et al., 2000). Some of the observed changes in CaT during acidosis are therefore likely to reflect changes in SR loading.

Fig. 3 shows that the time integral of inward I_{NCX}, triggered by unloading the SR with 20 mM caffeine (see Materials and methods), was reduced significantly by extracellular acidosis (−12%) but increased by intracellular (+25%) and combined acidosis (+123%). Intracellular acidification has been reported to have no effect on cytoplasmic Ca^{2+} buffering in rat ventricular myocytes (Choi et al., 2000), so changes in net I_{NCX} are likely to reflect changes in luminal SR load. Low pH_o therefore reduces luminal Ca^{2+}, whereas it is increased by low pH_i or combined low pH_i/pH_o.

Effect of acidosis on the $I_{Ca,L}$ I-V relationship

As the main source of Ca^{2+} influx in cardiac myocytes, $I_{Ca,L}$ serves as the trigger for SR Ca^{2+} release and helps maintain the plateau phase of the AP. We therefore examined the response of peak $I_{Ca,L}$ to each type of acidosis (left panels in Fig. 4, A–C). Reducing pH_i or pH_o had markedly different effects on the voltage dependence of $I_{Ca,L}$.

Extracellular acidosis decreased peak $I_{Ca,L}$ at nearly all voltages and shifted the I-V curve rightwards along the voltage axis, as indicated by the red arrow in Fig. 4 A (left). In contrast, intracellular acidosis shifted the I-V curve to the left (Fig. 4 B, left). This caused an increase in $I_{Ca,L}$ at voltages negative to 0 mV but a decrease at more positive voltages. Results for the combined acidosis protocol appeared to reflect the sum of the right and left shifts in the I-V relationship (Fig. 4 C, left). This produced control and acid I-V curves that were nearly superimposable at voltages negative to 0 mV, whereas $I_{Ca,L}$ remained lower than control at more positive potentials. Thus, although low pH_o is universally inhibitory on $I_{Ca,L}$, over an appropriate voltage range, low pH_i can be stimulatory, whereas these opposing effects tend to cancel when low pH_o and pH_i are applied simultaneously. Comparable responses to pH_i and pH_o were also seen in guinea pig ventricular myocytes (Fig. S3, A and B).

The opposing effects of pH_o and pH_i on peak $I_{Ca,L}$ are illustrated in Fig. 5, which quantifies pH sensitivity at a test voltage of −10 mV. Both plots are best-fitted with H^+ titration curves of similar pK (~6.9), but, at this test potential, the curve for pH_o is inhibitory, whereas that for pH_i is stimulatory. H^+ potency is thus comparable on both sides of the sarcolemma and expressed within the physiological pH range.

In other experiments (not depicted), $I_{Ca,L}$ measured with the perforated patch-clamp technique (amphotericin B) displayed similar pH_i sensitivity, indicating that results were not a function of intracellular dialysis during whole cell voltage clamp.

Effect of acidosis on the $I_{Ca,L}$ I-V relationship during BAPTA dialysis

$I_{Ca,L}$ is modulated (inhibited) by Ca^{2+} influx through the channel (Adachi-Akahane et al., 1996; Josephson et al., 2010), by SR Ca^{2+} release (Adachi-Akahane et al., 1996; Sham, 1997), and by a rise of $[Ca^{2+}]_{dia}$ (Kokubun and Irisawa, 1984; Tseng and Boyden, 1991; You et al., 1995). Because acidosis affects all these parameters, it is

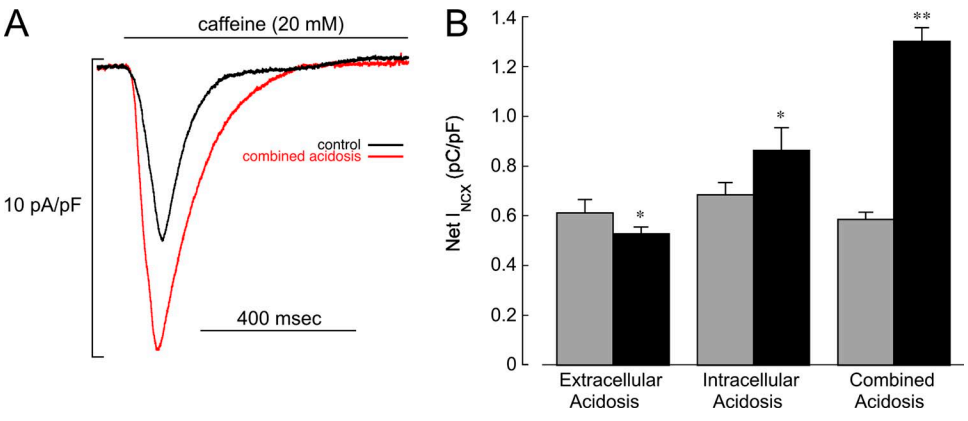

Figure 3. Acidosis and Ca^{2+} content of SR. (A) Specimen I_{NCX} signals recorded from a rabbit ventricular myocyte in response to rapid caffeine (20 mM) application during control and combined acidosis (2 min). The caffeine pulse was preceded by at least 15 conditioning AP-clamp pulses (CL = 2 s). The control and acidosis AP templates for the clamp pulses were the same as those used for $I_{Ca,L}$ measurements (Fig. 8). (B) Summary of integrated I_{NCX} demonstrating that extracellular acidosis ($n = 7$) decreased Ca^{2+} content, whereas intracellular ($n = 7$) and combined acidosis ($n = 6$) increased content. **, $P < 0.01$; *, $P < 0.05$, paired; control compared with 2 min of acidosis.

difficult to distinguish direct effects of H^+ ions on $I_{Ca,L}$ from indirect effects mediated via H^+-induced changes in cytosolic Ca^{2+}. We therefore repeated the I-V analysis of peak $I_{Ca,L}$ while including 5 mM BAPTA in the suction pipette (right panels in Fig. 4, A–C) to minimize displacements of Ca^{2+}_i. Fig. S4 confirms that BAPTA dialysis prevents both the CaT and the H^+-induced rise of $[Ca^{2+}]_{dia}$.

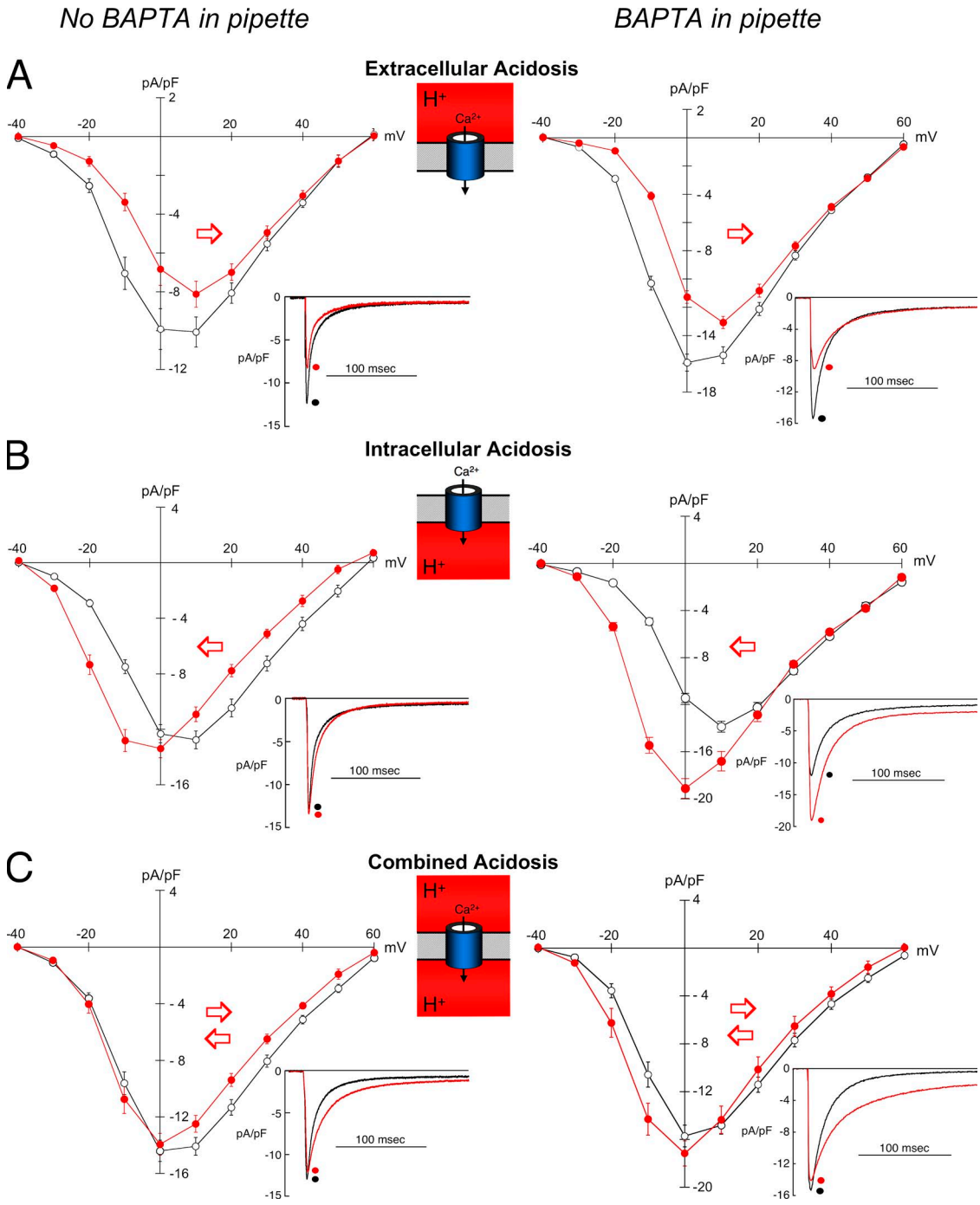

Figure 4. Acidosis and peak Ca^{2+} current. Effect of acidosis (red) on $I_{Ca,L}$ in the absence (left panels) and presence of BAPTA dialysis (right panels). Cells (rabbit) were held at −80 mV, and clamp steps were applied at CL = 5 s. (A; left) Extracellular acidosis without BAPTA dialysis (n = 6) depressed the I-V curve and shifted it to the right. (A; right) Extracellular acidosis with BAPTA dialysis (n = 13) had the same effect. (B; left) Intracellular acidosis without BAPTA dialysis (n = 14) shifted the curve to the left and slightly increased the peak. (B; right) Intracellular acidosis with BAPTA dialysis (n = 10) shifted the curve to the left and markedly increased peak $I_{Ca,L}$. (C; left) Combined acidosis without BAPTA dialysis (n = 10) had little effect on the I-V curve except inhibition at voltages positive to 0 mV. (C; right) Combined acidosis with BAPTA dialysis (n = 11) increased $I_{Ca,L}$ at voltages negative to −10 mV and caused somewhat less inhibition at more positive potentials. The example signals in each panel were obtained by clamping to 0 mV.

In rabbit myocytes, BAPTA dialysis had little effect on the inhibitory influence of low pH_o on peak $I_{Ca,L}$ (compare Fig. 4 A, left with right). With intracellular acidosis, however, the I-V curve was still left-shifted, causing stimulation of $I_{Ca,L}$ at negative voltages, but the inhibition seen previously at more positive voltages was now abolished (compare Fig. 4 B, left with right). Similar effects also occurred in guinea pig ventricular myocytes (compare Fig. S3, B with C). Thus, when inhibitory effects of Ca^{2+}_i are buffered out by BAPTA, the powerful stimulatory effect of intracellular acidosis on $I_{Ca,L}$ is more fully revealed.

Applying the combined acidosis protocol in the presence of BAPTA dialysis increased $I_{Ca,L}$ at all voltages (compare Fig. 4 C, left with right), but, as in the absence of BAPTA, the opposing effects of pH_i and pH_o tended to cancel. This resulted in less $I_{Ca,L}$ inhibition at voltages positive to 0 mV and only a modest stimulation at more negative potentials.

Collectively, the results demonstrate that the rise of diastolic Ca^{2+}_i at low pH_i normally exerts an important inhibitory influence on $I_{Ca,L}$. In the absence of the Ca^{2+}_i rise, intracellular acidosis is clearly stimulatory. This result is to be contrasted with extracellular acidosis, which, in the presence or absence of BAPTA dialysis, is inhibitory.

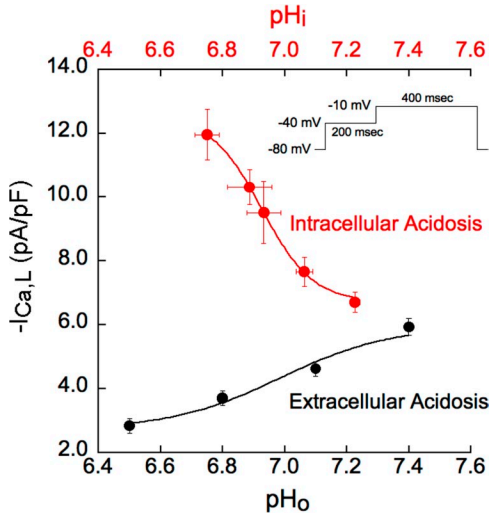

Figure 5. pH sensitivity of Ca^{2+} current. Quantitative relationship between $I_{Ca,L}$ and pH_o and pH_i in rabbit myocytes without BAPTA dialysis. The clamp step from −40 to −10 mV was chosen because, at this voltage, there were striking differences in the response of $I_{Ca,L}$ to pH_o and pH_i (Fig. 4, A and B). The magnitude of intracellular acidosis (pH_o 7.4) was varied by applying different concentrations of sodium acetate while keeping extracellular Ca^{2+} activity constant. The pH_i measurements were done in separate cells, with *n* values ranging from 5 to 13. The *n* values for $I_{Ca,L}$ measurements ranged from 5 to 14 for intracellular acidosis and from 7 to 16 for extracellular acidosis. $I_{Ca,L}$ was stimulated much more by intracellular acidosis (red) than it was suppressed by extracellular acidosis (black). Results for both types of acidosis fit with the equation: $-I_{Ca,L} = a + b/\{1 + [10^{(pK-pH)}]^n\}$ (Sabirov et al., 1997). The apparent pK values for these effects were comparable, 6.92 and 6.99, respectively, showing that the pH sensitivity of $I_{Ca,L}$ in both the extracellular and intracellular domains is strongly expressed over the physiological pH range.

pH sensitivity of $I_{Ca,L}$ is not caused by changes in Cl^- current

Acidosis has been reported to increase Ca^{2+}-activated Cl^- current in rabbit myocytes (Hirayama et al., 2002), which could potentially contaminate the present measurements of $I_{Ca,L}$. Fig. S3 D shows that the overall effects of intracellular acidosis on $I_{Ca,L}$ persisted in Cl^--free media (compare Fig. S4 D with Fig. 4 B, left). As noted above, a similar response to intracellular acidosis also occurred in guinea pig ventricular myocytes (Fig. S3 B), which are thought to lack Ca^{2+}-activated Cl^- current, except under conditions of Ca^{2+}_i overload (Nakajima et al., 2002). Collectively, the results suggest that possible contaminating effects of Cl^- current are unlikely to account for the observed changes in $I_{Ca,L}$.

Effect of acidosis on steady-state $I_{Ca,L}$ activation and inactivation

The results shown in Fig. 4 strongly suggest that H^+-induced changes in channel gating are causing the voltage shifts in the I-V curves. As discussed later, this may result from H^+ screening of, and/or binding to, anionic sites on the sarcolemma and Ca^{2+} channel protein (Kwan and Kass, 1993; Hille, 2001). The effects of each type of acidosis on steady-state activation (d_∞) and inactivation (f_∞) of $I_{Ca,L}$ are illustrated in Fig. 6. The experiments were performed without BAPTA dialysis. Tables S1 and S2 summarize the values for $V_{1/2}$, G_{max}, k, and V_{rev} shown in Fig. 6. In agreement with earlier work in guinea pig ventricular myocytes (Krafte and Kass, 1988; Kwan and Kass, 1993), exposure of rabbit myocytes to extracellular acidosis induced a right shift in $V_{1/2}$ for both activation and inactivation (Fig. 6 A). In contrast, intracellular acidosis shifted both curves to the left, although by somewhat different amounts (Fig. 6 B). Combined acidosis nearly cancelled out the individual actions of low pH_i and pH_o, by shifting both curves back toward their control values (Fig. 6 C). This pattern of voltage shift in d_∞ and f_∞, induced by the three types of acidosis, was preserved during BAPTA dialysis (Tables S1 and S2). The findings demonstrate that intracellular and extracellular acidosis exert opposing effects on the voltage dependence of channel gating.

Effect of acidosis on the time course of $I_{Ca,L}$ inactivation

The kinetics of $I_{Ca,L}$ inactivation were also affected by acidosis. Inactivation is normally both voltage dependent (voltage-dependent inactivation [VDI]) and Ca^{2+}_i dependent (calcium-dependent inactivation [CDI]) (Kass and Sanguinetti, 1984; Lee et al., 1985; Yue et al., 1990; Adachi-Akahane et al., 1996; Sham, 1997; Cens et al., 2006).

The time course of current inactivation can be characterized by fast (τ_f) and slow (τ_s) time constants (Isenberg and Klöckner, 1982; Sun et al., 1997).

Fig. 7 plots τ_f and τ_s for each type of acidosis over the "plateau range" of voltages (i.e., 0 to +30 mV), measured without BAPTA dialysis. Additional inactivation parameters, $A_f/(A_f + A_s)$ and C, are presented in Table S3. Extracellular acidosis speeded up slightly the time course of $I_{Ca,L}$ inactivation (Fig. 7 A), although this reached statistical significance only at the more positive voltages. In contrast, low pH_i and combined pH_i/pH_o slowed inactivation at almost all voltages tested (Fig. 7, B and C). When changes of $Ca^{2+}{}_i$ were suppressed by BAPTA dialysis, the time course of current inactivation was slowed under control, nonacidic conditions (Table S4), as reported previously (Josephson et al., 1984; Lacinová and Hofmann, 2005), but now all three types of acid challenge slowed $I_{Ca,L}$ inactivation, most particularly the combined acidosis (Fig. S5).

The results demonstrate that, over the plateau range of AP voltages, acidosis directly slows $I_{Ca,L}$ inactivation. It can therefore enhance Ca^{2+} influx during the inactivating phase of the current. To unmask the full extent of this enhancement, however, the inhibitory action of increases in $Ca^{2+}{}_i$ during acidosis (which speed up $I_{Ca,L}$ inactivation) must be suppressed with BAPTA dialysis.

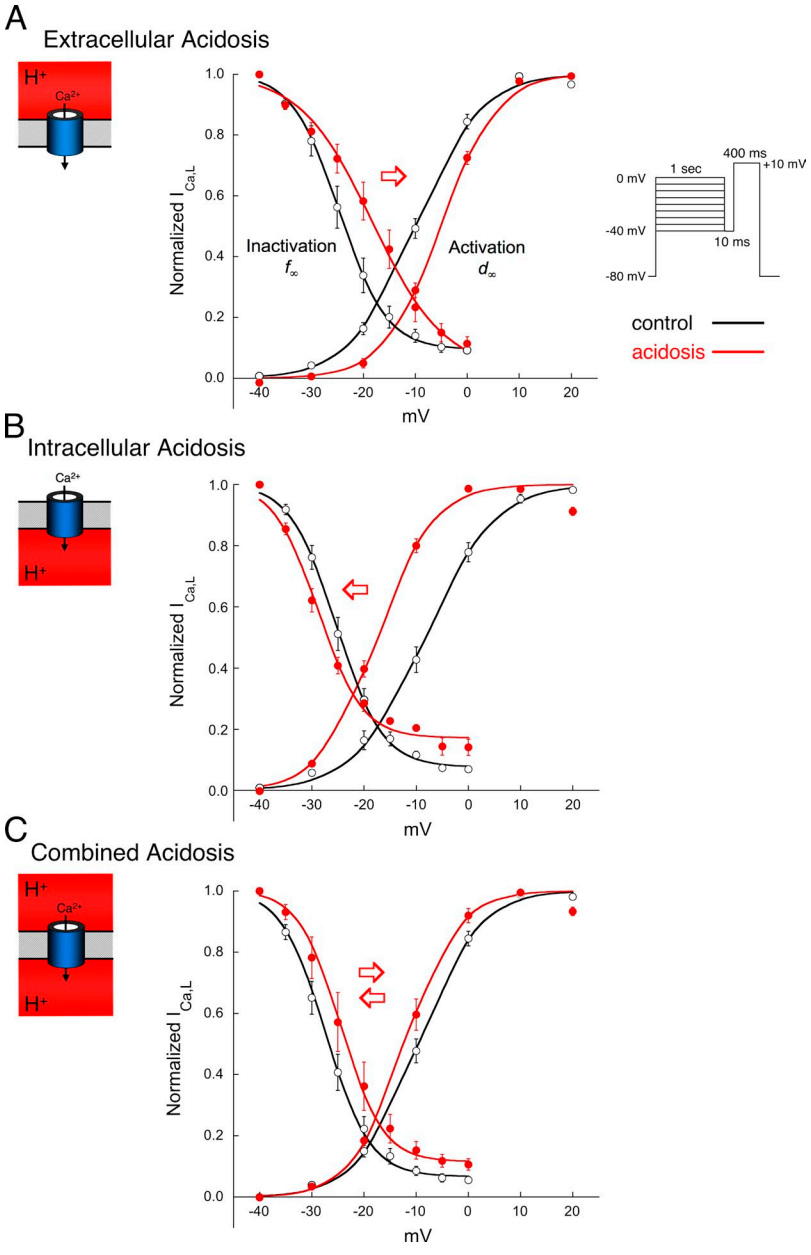

Figure 6. Acidosis and Ca^{2+} current gating. Effect of acidosis on the voltage dependence of rabbit $I_{Ca,L}$ activation and inactivation. The voltage-clamp protocol for inactivation is shown in the inset. The clamp protocol for activation is given in Materials and methods, and the smooth lines are best fits with Boltzmann functions. The normal pipette filling solution (no BAPTA) was used in all experiments shown in this figure. The clamp protocols were applied first in the control solution (black), then after 2 min in the acidic solutions (red). Tables S1 and S2 summarize the parameters for the curves shown in this figure. (A) Extracellular acidosis (n = 6) elicited right shifts in both activation and inactivation curves. (B) Intracellular acidosis (n = 13) shifted both curves to the left, with a larger shift in activation. (C) Combined acidosis (n = 11) shifted both curves back to the right compared with intracellular acidosis.

Effect of acidosis on net Ca^{2+} influx via $I_{Ca,L}$

To determine if acidosis affects net Ca^{2+} entry via $I_{Ca,L}$, we integrated the time course of $I_{Ca,L}$ signals (rabbit myocytes) elicited by a 400-msec clamp step from −40 to +20 mV (Fig. 4), a test voltage that approximates the voltage midrange of the AP plateau (Fig. 1). In the absence of BAPTA dialysis, low pH_o decreased net Ca^{2+} entry, whereas intracellular and combined acidosis increased it. The respective changes were from 0.34 ± 0.02 to 0.31 ± 0.02 pC/pF (n = 7; P < 0.05, paired) for extracellular acidosis, from 0.37 ± 0.04 to 0.49 ± 0.05 pC/pF (n = 11; P < 0.01, paired) for intracellular acidosis, and from 0.41 ± 0.04 to 0.66 ± 0.08 pC/pF (n = 11; P < 0.01, paired) for combined acidosis. Qualitatively, this pattern of net entry also occurred at +10 mV. Thus, low pH_o and low pH_i exert opposite effects on net Ca^{2+} entry (inhibition and stimulation, respectively).

With BAPTA in the pipette to minimize H^+-induced changes in Ca^{2+}_i, both intracellular and combined acidosis again increased net Ca^{2+} entry. The respective increases were from 0.54 ± 0.5 to 1.24 ± 0.8 pC/pF (n = 10; P < 0.001, paired) for intracellular acidosis and from 0.56 ± 0.5 to 1.16 ± 0.9 pC/pF (n = 10; P < 0.001, paired) for combined acidosis. In contrast, extracellular acidosis did not significantly change net charge entry (n = 13; paired). This resulted from the counteracting actions of extracellular acidosis at +20 mV to reduce initial peak I_{CaL} (Fig. 4 A, right) but slow its subsequent inactivation (Fig. S5 A). Qualitatively, the same pattern of net entry also occurred at +10 mV for each type of acidosis.

In summary, during a voltage-clamp depolarization, low pH_i increases net Ca^{2+} entry via the L-type Ca^{2+} channel, whereas low pH_o reduces it (except with BAPTA dialysis, when there is no effect).

Effect of pH on L-type channel gating with Na^+ instead of Ca^{2+} as the charge carrier

The sensitivity of current flow through the L-type Ca channel was also investigated using Na^+ instead of Ca^{2+} as the charge carrier (superfusates were Ca^{2+} free). This

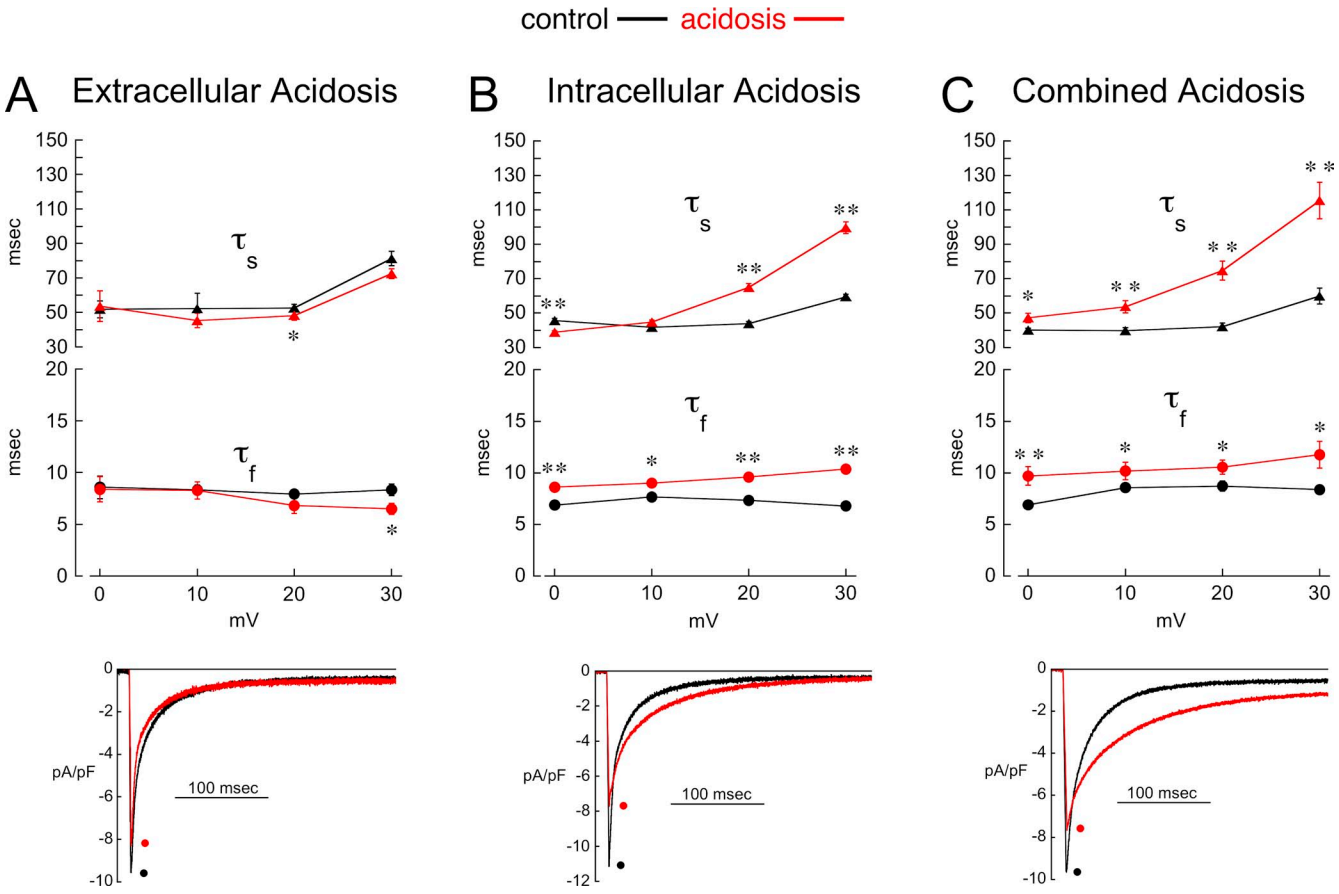

Figure 7. Acidosis and Ca^{2+} current inactivation kinetics. Effect of acidosis on the voltage dependence of $I_{Ca,L}$ inactivation kinetics. Cells (rabbit) were voltage clamped according to the protocol shown in Fig. 3 (CL = 5 s). τ_f and τ_s were measured as described in Materials and methods, with all acidic results shown in red. The normal pipette filling solution (no BAPTA) was used in all experiments shown in this figure. (A) Extracellular acidosis (n = 6) had little effect on inactivation kinetics. (B) In contrast, intracellular (n = 14) acidosis slowed both τ_f and τ_s over most of the voltage range. (B) Combined acidosis (n = 6) caused the greatest slowing of inactivation. **, P < 0.01; *, P < 0.05, paired; control compared with 2 min of acidosis. The example records were recorded from three different cells in response to a clamp step from −40 to +20 mV.

approach removes the complicating effects on $I_{Ca,L}$ of changes in Ca^{2+}_i (Na^+ exerts no modulatory effect on L-type channel inactivation). Data are summarized in Fig. S6 and strongly resemble results obtained above with Ca^{2+}. For example, low pH_o inhibited peak current through the channel, whereas low pH_i stimulated it. In addition, both types of acidosis slowed the time course of channel inactivation (both the fast and slow components), similar to results seen above with BAPTA dialysis when using Ca^{2+} as the charge carrier. The results therefore provide further confirmation of the opposing effects of H^+_i and H^+_o on L-type channel gating. They also demonstrate that acidosis must directly slow VDI of the channel, as CDI is not operational when using Na^+ as the charge carrier.

Effect of acidosis on $I_{Ca,L}$ during AP clamps

To determine the effects of acidosis on $I_{Ca,L}$ under more physiological conditions than with conventional voltage-clamp pulses, we performed AP-clamp experiments (Fig. 8). Fig. 1 showed that APD was shortened by extracellular acidosis, whereas intracellular and combined acidosis elevated the plateau and prolonged APD. These AP trajectories were used as templates for the AP clamp (see Materials and methods for experimental details).

Extracellular acidosis in combination with the corresponding AP template reduced peak $I_{Ca,L}$ (by −14%) and net Ca^{2+} influx (by −23%) measured during the course of the AP (Fig. 8 B, a and b). When the control and low pH_o AP templates were applied in normal

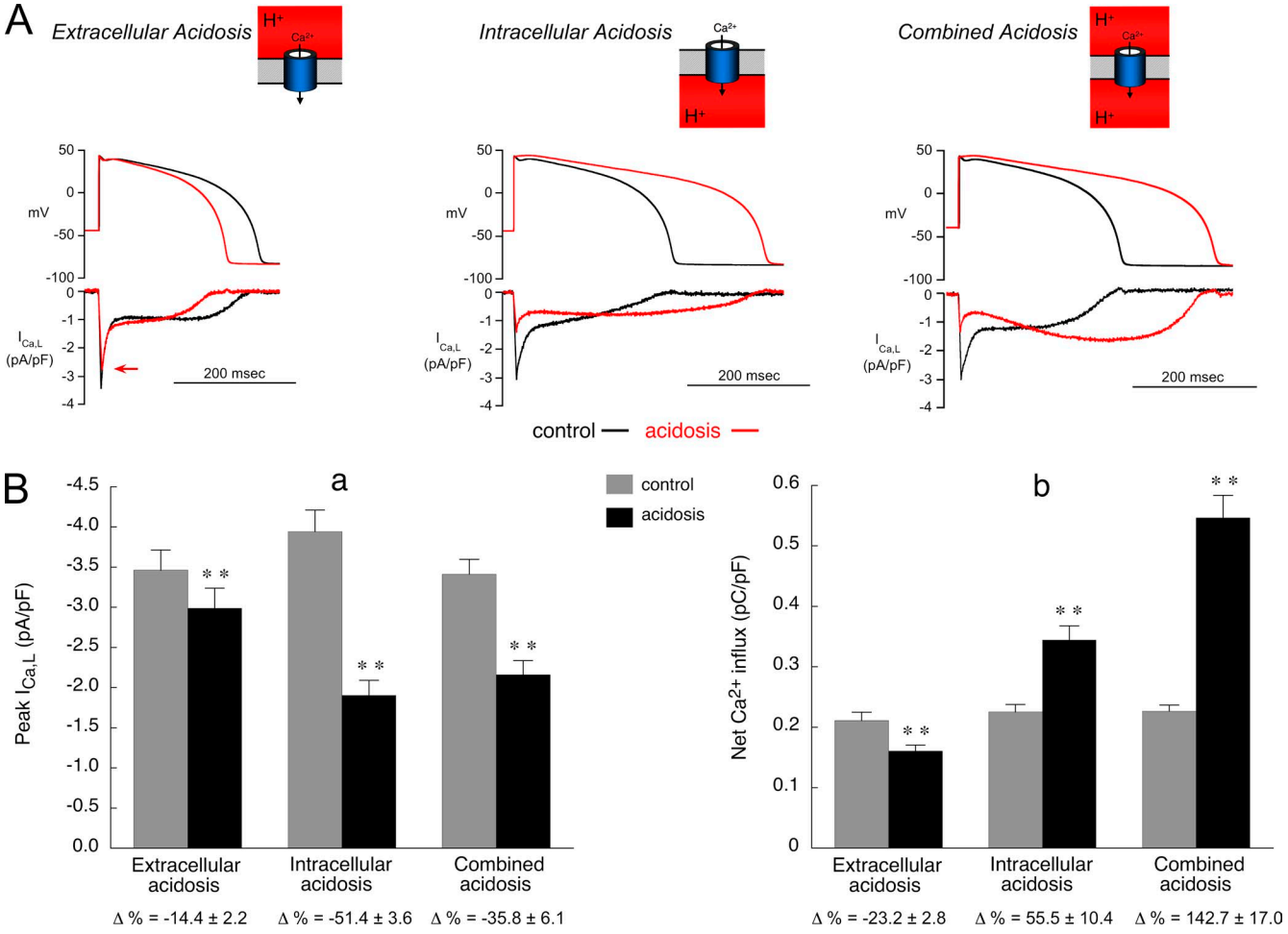

Figure 8. Acidosis and Ca^{2+} current during an AP. Effect of acidosis on rabbit $I_{Ca,L}$ during AP voltage clamps. The normal pipette filling solution (no BAPTA) was used in all experiments shown in this figure. The voltage templates used for control and acidosis are representative of APs recorded at a CL of 2 s during the three types of pH displacement. The same control AP waveform was used for each type of acidosis, and the same acidic AP waveform was used for both intracellular and combined acidosis. (A) Representative examples of AP clamps in control solution (black) and after 2 min of acidosis (red). Each type of acidosis reduced the initial peak value of $I_{Ca,L}$. The red arrow in the extracellular acidosis panel (left) indicates the initial peak $I_{Ca,L}$ during acidosis. (B; a) Summary of results for initial peak amplitude of $I_{Ca,L}$ (extracellular acidosis, $n = 12$; intracellular acidosis, $n = 12$; combined acidosis, $n = 7$). **, control versus acidosis; $P < 0.01$, paired. (b) Summary of results for net Ca^{2+} influx showing that extracellular acidosis decreased influx while the other types of acidosis increased influx. *n* values and statistics are the same as in B (a).

(nonacidotic) solution (not depicted), there was no significant change in initial peak $I_{Ca,L}$ (−1.1 ± 0.9%; n = 5) and only a modest decrease in net Ca^{2+} entry (−12.2 ± 3.3%; n = 5; paired, P < 0.05). Thus, much of the decrease in peak current and net Ca^{2+} entry is a result of the acidosis rather than the attendant change in AP configuration.

Intracellular or combined acidosis in combination with the corresponding AP template induced larger reductions in initial peak $I_{Ca,L}$ (up to −51%) and greatly increased net Ca^{2+} influx (up to 142%; Fig. 8 B, a and b). Previous work has shown that the slowing of phase 1 repolarization under nonacidotic conditions decreases peak $I_{Ca,L}$ (Sah et al., 2003), whereas elevation of the AP plateau in rabbit and guinea pig ventricular myocytes also decreases peak $I_{Ca,L}$ and slows inactivation (Linz and Meyer, 2000). In the present work, however, applying the prolonged low pH_i AP template in rabbit myocytes, but without intracellular or combined acidosis, had no significant effect on initial peak $I_{Ca,L}$ (−4.1 ± 2.8%) and induced a much smaller increase in net Ca^{2+} entry (by 17.5 ± 2.1%; n = 5; paired, P < 0.05). Thus, as with low pH_o, most of the peak and net Ca^{2+} current change observed with intracellular or combined acidosis during the AP clamps was caused by the pH rather than the AP change. It remains possible, nevertheless, that peak $I_{Ca,L}$ may be reduced more in cells that express a larger I_{to} density, as these will exhibit a greater slowing of phase 1 repolarization.

As shown in Fig. S7, we also performed AP-clamp experiments with intracellular BAPTA dialysis to minimize the complicating influence on $I_{Ca,L}$ of acid-induced

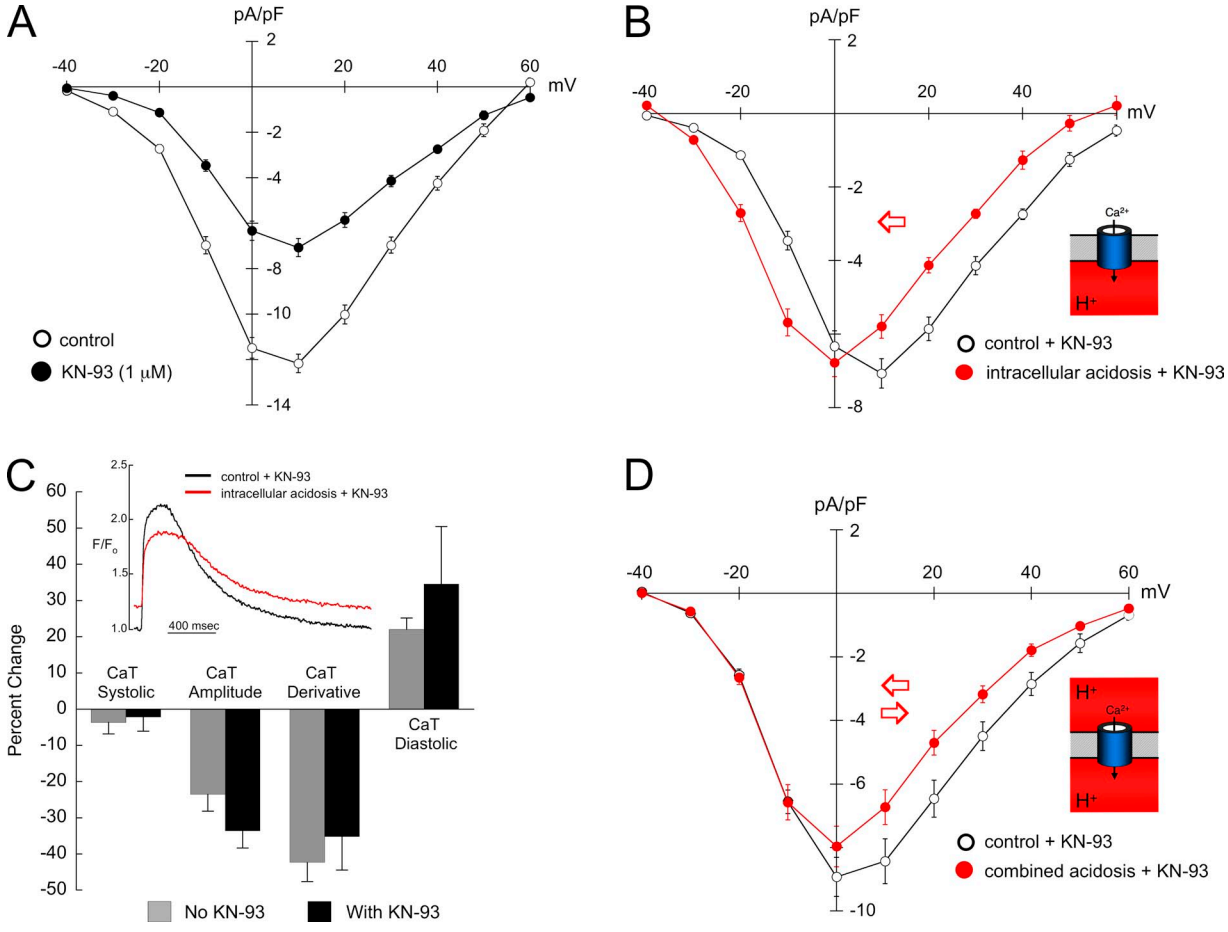

Figure 9. Acute pH sensitivity of Ca^{2+} current and CaT unaffected by CaMKII inhibition (rabbit myocytes). The normal pipette filling solution (no BAPTA) was used in all voltage-clamp experiments shown in this figure. (A) 1 μM KN-93 reduced $I_{Ca,L}$ under control conditions (pH_o 7.4): control, n = 26; KN-93, n = 8. The voltage-clamp protocol used for the KN-93 experiments was identical to that used to generate the results in Fig. 4 (CL = 5 s). (B) In the presence of 1 μM KN-93, intracellular acidosis shifted the I-V curve to the left (red arrow), with no change in the peak (n = 8), the same response observed without KN-93 (compare Fig. 4 B, left). (C) Summarized effects of intracellular acidosis (2 min) on CaT characteristics in the presence (n = 5) and absence (n = 12) of 1 μM KN-93, expressed as percent change. Cells were field stimulated at CL = 2 s. There was no significant difference between the two groups (unpaired). Inset shows example CaTs from a myocyte in KN-93 during control and after 2 min of intracellular acidosis. (D) Effect of combined acidosis on $I_{Ca,L}$ in the presence of 1 μM KN-93 (n = 8). The response to combined acidosis was very similar to that without KN-93 (compare Fig. 4 C, left).

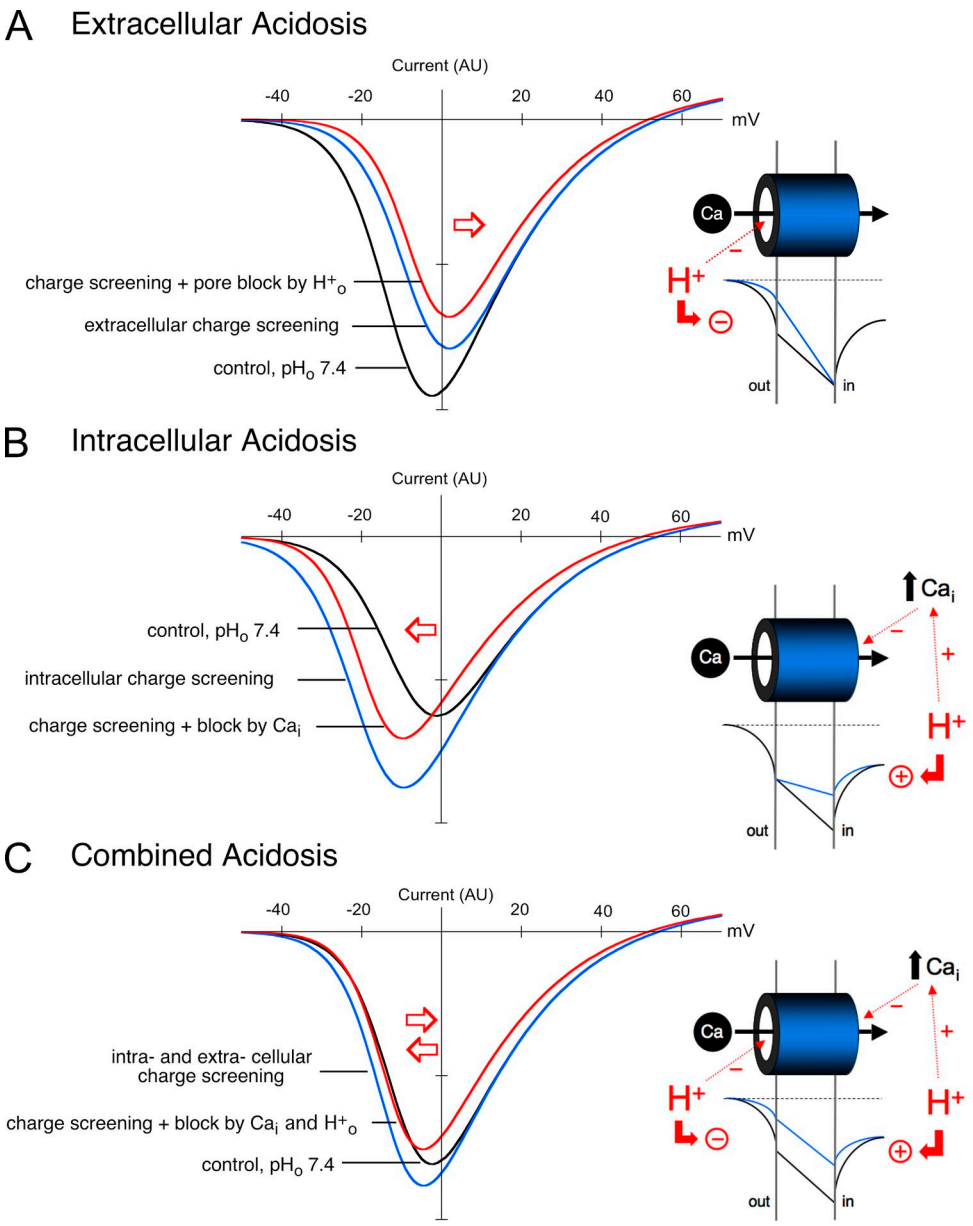

Figure 10. Modeling acidosis on the I-V curve for peak $I_{Ca,L}$. To simulate the overall effects of acidosis on the I-V curve, we used the mean activation parameters ($V_{1/2}$, k) shown in Table S1 (without BAPTA) and a modification of the equation of Hanck and Sheets (1992), $I_{Ca,L} = G_{max}(V_m - V_{rev})/[1+\exp(V_m - V_{1/2})]/k$, as a simplified model for the voltage dependence of peak $I_{Ca,L}$. The term, $G_{max}(V_m - V_{rev})$, was replaced by a GHK equation for $I_{Ca,L}$, similar to that described by Luo and Rudy (1994):

$$\bar{I}_{Ca,L} = \bar{I}_{Ca} + \bar{I}_{Cs}$$

$$\bar{I}_s = P_s\, z_s^2\, V_m\, \frac{F^2}{RT}\, \frac{[S]_i \exp(z_s\, V_m\, F)/(RT) - [S]_o}{\exp(z_s\, V_m\, F)/(RT) - 1},$$

where $\bar{I}_{Ca,L}$ is the sum of peak current carried by calcium ($\bar{I}_{Ca,L}$) and cesium ($\bar{I}_{Cs}$), and z, F, R, and T have their usual meanings. P_{Ca} under control conditions was taken as 5.4×10^{-4} cm/sec, and P_{Cs} was assumed to be similar to P_K at 2.7×10^{-7} cm/sec (Lou and Rudy, 1994). $[Ca^{2+}]_o$ was 1.1 mM and $[Ca^{2+}]_i$ was assumed to be 100 nM under control conditions. Raising $[Ca^{2+}]_i$ to as high as 1 µM has a negligible effect on the calculated $I_{Ca,L}$ reversal potential, so $[Ca^{2+}]_i$ was kept at 100 nM in all simulations. $[Cs^+]_i$ was assumed to be equal to that in the pipette at 133 mM, and $[Cs^+]_o$ was 4.4 mM. The results for each type of acidosis simulation are summarized in each panel. The cartoon figures depict qualitatively the effects of each type of acidosis on the voltage profile within the sarcolemma (black, control; blue, acidosis) and channel permeability. A larger sarcolemmal surface potential is shown on the inner membrane surface in accord with previous reports in cardiac cells (Post et al., 1988). All calculations in this figure were made according to Eqs. 2 and 3. The control-simulated I-V curves in all panels are shown in black. (A) Extracellular acidosis. Shifting the $V_{1/2}$ of activation (d_∞) by the measured amount of 48.5% to the right moved the curve downward and to the right (blue), as indicated by the red arrow. Also included is the measured

changes in $[Ca^{2+}]_i$, and to remove any contaminating influence of Ca^{2+}-activated changes in I_{NCX} (see Materials and methods). Initial peak $I_{Ca,L}$ was again decreased by low pH_o. In contrast, low pH_i or combined acidosis exerted no inhibitory effect on peak current, indicating that much of the decrease observed in the absence of BAPTA is a result of secondary effects of Ca^{2+}_i elevation. Inspection of net Ca^{2+} entry during the AP indicates, again, that it was reduced by low pH_o but greatly enhanced by low pH_i or combined acidosis, a result very similar to that seen in the absence of BAPTA dialysis. Thus, even when Ca^{2+}_i changes are buffered, net Ca^{2+} entry during an AP is reciprocally controlled by pH_o and pH_i.

Effect of CaMKII inhibition on acid-induced changes in $I_{Ca,L}$ and CaT

Previous studies using the CaMK inhibitor, KN-93, have proposed a role for this enzyme in stimulating $I_{Ca,L}$, SR calcium uptake, CaTs, and contraction in ventricular myocytes during acidosis (Komukai et al., 2001; Nomura et al., 2002; DeSantiago et al., 2004; Mattiazzi et al., 2007). It is important to note that, although KN-93 inhibits CaMKs, it has also been shown to inhibit L-type calcium channels in a CaMKII-independent manner (Gao et al., 2006). To determine if CaMK activity contributed to our results, and for purposes of comparison with previous work, we subjected rabbit myocytes to 2 min of intracellular or combined acidosis in the presence of 1 µM KN-93 (Fig. 9). Cells were equilibrated for at least 15 min with the drug before beginning the experiment.

In accord with earlier work in rat ventricular myocytes (Komukai et al., 2001), KN-93 significantly reduced $I_{Ca,L}$ in rabbit myocytes under normal nonacidic conditions (Fig. 9 A), but the effect of low pH_i on the I-V curve for peak $I_{Ca,L}$ (compare Fig. 9 B with Fig. 4 B, left) and on electrically evoked CaTs was unaffected (Fig. 9 C). With a combined acidosis, KN-93 slightly increased the inhibition of peak $I_{Ca,L}$ normally observed at positive voltages (compare Fig. 9 D with Fig. 4 C, left), from 8% inhibition at +10 mV and 17% at +30 mV under control conditions, to 11 and 21%, respectively, in the presence of KN-93. Collectively, the results show that the acute pH sensitivity of $I_{Ca,L}$ reported in the present work is essentially the same with or without CaMKII activity.

DISCUSSION

This work reveals effects of pH on the cardiac ventricular $I_{Ca,L}$ and AP (guinea pig and rabbit), which differ radically from previous reports. Although extracellular H^+ ions inhibit the Ca^{2+} current, as documented previously, intracellular H^+ ions can be stimulatory. These different effects are partly the result of an opposing influence of H^+_i and H^+_o ions on the voltage dependence of L-type channel activation. An additional action of H^+ ions is to slow the kinetics of channel inactivation, which, during intracellular or combined acidosis, enhances net Ca^{2+} entry during the plateau phase of the cardiac AP, thereby prolonging it. Unraveling these complex effects has depended on the experimental manipulation of both pH_i and pH_o. But it has also depended on the recognition that acidosis elevates diastolic Ca^{2+} in ventricular myocytes, which has a secondary inhibitory influence on $I_{Ca,L}$. This sometimes obscures the more direct H^+ ion effect. The combined influence of pH and Ca^{2+}_i on $I_{Ca,L}$ can now be used to reconstruct the effect of an acid–base disturbance on electrical and Ca^{2+} signaling. Results of this indicate that pH modulation of $I_{Ca,L}$ is likely to provide an important link between myocardial metabolism that generates H^+ ions and cardiac function that is H^+ sensitive.

pH control of $I_{Ca,L}$: Peak $I_{Ca,L}$

Peak $I_{Ca,L}$ is the principal trigger for SR Ca^{2+} release and subsequent contraction in ventricular myocytes. Our results suggest multiple modes of H^+ action on this current.

Extracellular acidosis. With low pH_o, the reduction in peak $I_{Ca,L}$ was evident regardless of whether bulk Ca^{2+}_i

13.6% reduction in k, which had only a small effect on the curve. The red curve includes the same changes in $V_{1/2}$ and k, along with a 16.6% reduction in P_{Ca}. The latter was obtained by systematically varying P_{Ca} until the percent drop in current at 0 mV, compared with control, matched the 30% decline measured experimentally (Fig. 4 B, left). The cartoon depicts qualitatively the actions of external protons to both decrease P_{Ca} (dashed red arrow) and screen/bind external surface charge (red circle with "−" and blue lines in membrane). (B) Intracellular acidosis. Shifting the $V_{1/2}$ of activation by the measured amount of −112.0% to the left moved the curve upward and to the left (blue), as indicated by the red arrow. Also included is the measured 20.0% reduction in k, which had only a small effect on the curve. The red I-V curve includes the same changes in $V_{1/2}$ and k, along with a 24.0% reduction in P_{Ca}. The latter was obtained by systematically varying P_{Ca} until the percent drop in current at +20 mV, compared with control, matched the 26% current decline measured experimentally (Fig. 4 B, left). The cartoon illustrates qualitatively the actions of intracellular protons to increase $[Ca^{2+}]_i$ and screen/bind internal surface charge (red circle with "+" and blue lines in membrane). It also shows the action of increased $[Ca^{2+}]_i$ to decrease channel permeability (dashed red arrow). (C) Combined acidosis. A left shift in the $V_{1/2}$ of activation by the measured amount of 24.7% moved the curve upward and to the left (blue). Also included is the 11.1% decrease in k, which had only a small effect on the curve. The red curve includes the same changes in $V_{1/2}$ and k, along with a 16.6% reduction in P_{Ca}. The latter was obtained by systematically varying P_{Ca} until the percent drop in current at +20 mV, compared with control, matched the 17% current decline measured experimentally (Fig. 4 C, left). The cartoon illustrates qualitatively the proposed actions of combined acidosis on $[Ca^{2+}]_i$, channel permeability, and the voltage drop across the sarcolemma (blue lines in membrane).

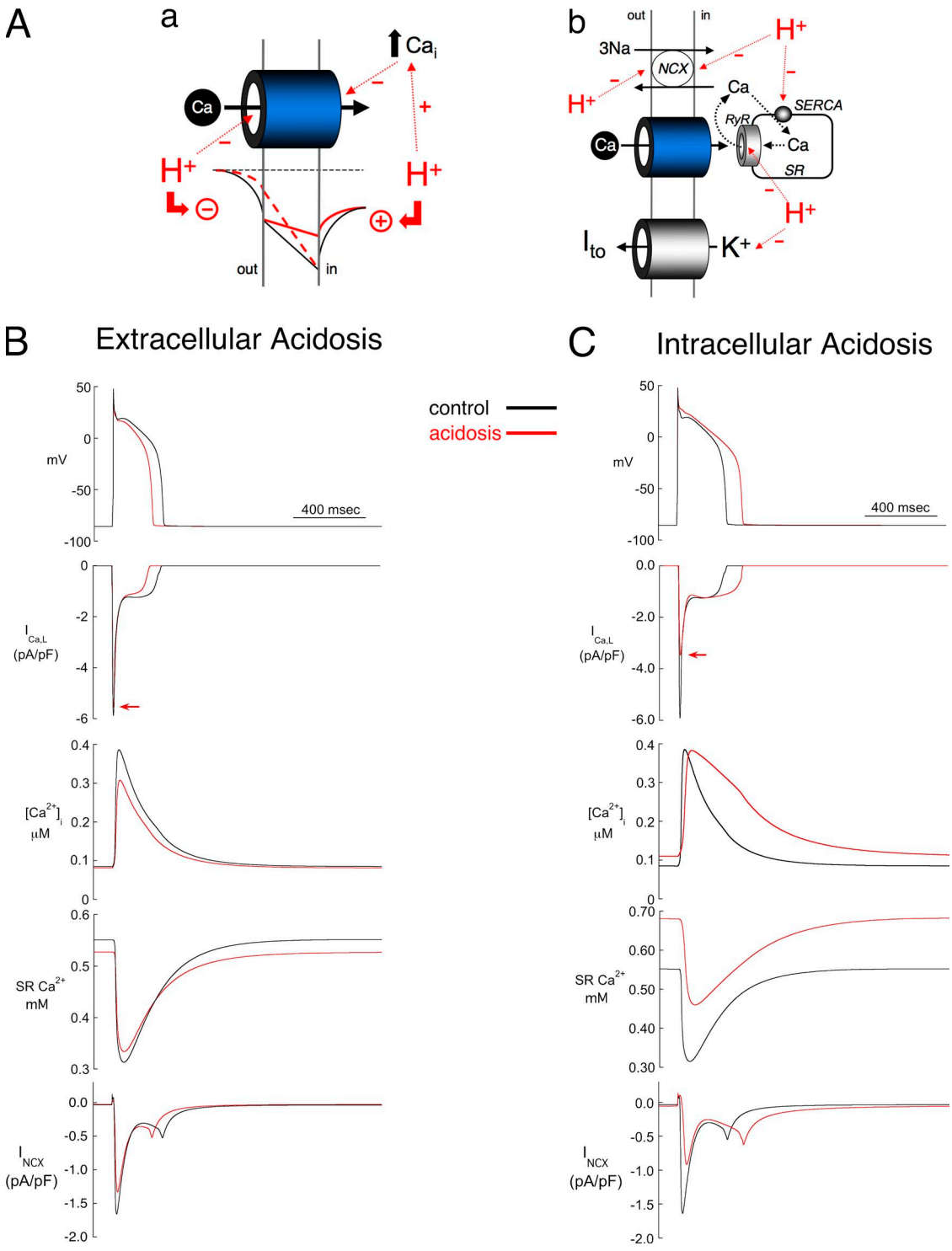

Figure 11. Modeling acidosis on Ca^{2+} signaling and the AP (rabbit ventricular myocyte). All simulations were performed using the computational model of Shannon et al. (2004) for Ca^{2+} handling and ionic currents in the rabbit ventricular myocyte. The control parameters and code for the model were obtained from version 1.6.91 on the JSim website, developed as part of the Physiome Project. The model was paced at 0.5 Hz for 2 min for both simulations. (A; a) The simulations include the separate actions of H^+_o and H^+_i to modulate charge screening/binding of surface charge and P_{Ca} as described in Fig. 10 (A and B). Not depicted in the cartoon, but included in the simulations (C), is the action of intracellular acidosis to slow $I_{Ca,L}$ inactivation. (b) The simulations also included additional inhibitory effects of H^+ on NCX, SR Ca^{2+} release channels (RyR), SERCA, and transient outward current (I_{to}). (B) The simulated effects of extracellular acidosis on APD, $I_{Ca,L}$, CaT, SR Ca^{2+}, and I_{NCX} were achieved by a 17% reduction in P_{Ca} (Fig. 10 A) and included the measured changes in $V_{1/2}$ and k for d_∞ and f_∞ (Tables S1 and S2; no BAPTA). In addition, I_{NCX} was reduced by 15% to simulate the actions of external protons on NaCa exchange (Egger and Niggli, 2000). All other parameters were set to default values. (C) The simulated

was clamped by intracellular BAPTA (Fig. 4 A) and so is independent of changes in Ca^{2+}_i. The inhibition agrees with earlier measurements in guinea pig ventricular myocytes, albeit made at room temperature and without NHE inhibition (Krafte and Kass, 1988; Kwan and Kass, 1993). At least two mechanisms have been proposed: (1) alterations in channel gating by H^+ screening of anionic sites on the sarcolemma and/or the Ca^{2+} channel protein (Kwan and Kass, 1993; Hille, 2001), and (2) direct H^+ ion blockade of the channel pore itself (X.H. Chen et al., 1996; Chen and Tsien, 1997). Although our experiments cannot resolve the relative importance of local sarcolemmal charge screening versus binding to the channel protein, a combination of mechanisms is likely to contribute to the full profile of $I_{Ca,L}$ inhibition.

By titrating negative charge local to the membrane, extracellular H^+ ions may effectively increase the voltage gradient experienced by the channel protein. This phenomenon, first described for the action of extracellular divalent cations on Na^+ current in nerve (Frankenhaeuser and Hodgkin, 1957) and later for pH_o on Ca^{2+} current in heart (Kwan and Kass, 1993), is illustrated in the cartoon shown in Fig. 10 A. In the case of low pH_o, a larger membrane depolarization is now required for channel activation, thus accounting for the right-shifted activation curve (Fig. 6) and hence the inhibitory effect on peak $I_{Ca,L}$ (Fig. 4 A). The simultaneous influence of charge screening on channel inactivation will exert a negligible effect at peak $I_{Ca,L}$, as inactivation is slow to develop. The specific nature of the negative charges to be screened, such as carboxyl or amine/imidazole residues, is not identified in our experiments, but their mean pK would appear to be ∼6.9 (see Fig. 5). The screening effect is reproduced in the mathematical simulation shown in Fig. 10 A. The shift in $V_{1/2}$ measured for steady-state activation (Fig. 6 A and Table S1) has been used to model the voltage dependence of peak $I_{Ca,L}$ before and during acidosis (Fig. 6 A, black vs. right-shifted blue line). Note that, at extreme positive voltages, full activation of Ca^{2+} channels is still achieved in low pH_o, so there is no change in the I-V relationship predicted in this region.

Extracellular H^+ ions can also block the Ca^{2+} channel pore directly (X.H. Chen et al., 1996; Chen and Tsien, 1997). By reducing the available population of L-type Ca^{2+} channels, extracellular acidosis decreases maximal sarcolemmal Ca^{2+} permeability, P_{Ca}. When incorporated into the computational model, this decrease predicts a reduction in $I_{Ca,L}$ across the entire voltage range. Fig. 10 A (red line) shows that a 16.6% reduction of P_{Ca}, when combined with the rightward shift in channel activation, produces a good approximation to the overall I-V curve observed experimentally during extracellular acidosis (compare Fig. 4 A). Thus, the effects of extracellular acidosis on $I_{Ca,L}$ are consistent with a dual H^+ inhibition of Ca^{2+} channels induced by a positive shift in channel gating and a direct block of the channel pore.

Intracellular acidosis. Effects of intracellular acidosis are strikingly different from those of extracellular acidosis. When changes of Ca^{2+}_i are prevented by BAPTA dialysis, a rise of intracellular H^+ ions is stimulatory, not inhibitory. This is best illustrated in Figs. 4 B (right), where reducing pH_i enhanced peak $I_{Ca,L}$ in rabbit myocytes over the voltage range of −40 to +20 mV (similar results in guinea pig myocytes; see Fig. S3 C). Thus, contrary to previous reports, acidosis can stimulate $I_{Ca,L}$, provided it is exclusively intracellular.

The left shift in steady-state channel activation during intracellular acidosis (Fig. 6 B) suggests that negative charge screening/binding by H^+ ions may be occurring at the inner sarcolemmal surface (again with a mean pK of ∼6.9; see Fig. 5). Unlike extracellular acidosis, this would be expected to decrease the local voltage gradient experienced by the Ca^{2+} channel, thus increasing its excitability (the left shift in channel activation; Fig. 6 B), thereby stimulating peak $I_{Ca,L}$, as shown in Fig. 4 B and illustrated in the schematic cartoon of Fig. 10 B. By using the experimentally measured channel activation parameters (Table S1), the left shift in the I-V curve is simulated well by the computational model (from the black control trace to the blue trace in Fig. 10 B).

When H^+-induced changes of Ca^{2+}_i occurred (i.e., with no intracellular BAPTA dialysis), enhancement of peak $I_{Ca,L}$ during intracellular acidosis was still evident at negative test potentials, but inhibition occurred at more positive voltages (Figs. 4 B, left, and S3 B). This inhibition was secondary to the rise of diastolic Ca^{2+}, as it was removed by BAPTA dialysis. Several studies have shown that a rise in diastolic Ca^{2+} decreases $I_{Ca,L}$ in both ventricular and Purkinje myocytes (Kokubun and Irisawa, 1984; Tseng and Boyden, 1991; You et al., 1995; Höfer et al., 1997), most likely by promoting tonic channel

effects of intracellular acidosis on APD, $I_{Ca,L}$, CaT, SR Ca^{2+}, and I_{NCX} were achieved by a 24% reduction in P_{Ca} (Fig. 10 B) and applying the measured changes in $V_{1/2}$ and k for d_∞ and f_∞ (Tables S1 and S2; no BAPTA). Additional changes included: (a) 1.2-fold increase in the time constant of $I_{Ca,L}$ inactivation (τ_f) to simulate slowing of inactivation (Fig. 7); (b) 40% reduction in SERCA pump rate (Kentish and Xiang, 1997); (c) a 40% reduction in SR calcium release flux (RyR activity) (Xu et al., 1996); and (d) a 20% reduction in I_{NCX} (Doering et al., 1996). In addition, both the slow and fast components of transient outward current were reduced by 50% in accord with our experimental findings in rabbit ventricular myocytes (Saegusa, N., V. Garg, and K.W. Spitzer. 2011. Transient outward current responds differently to external and internal protons in ventricular myocytes. Heart Rhythm Society Meeting. Abstr. S252). All other parameters were set to default values.

inactivation (You et al., 1997). This form of inhibition during low pH_i can be approximated in the computational model by scaling down P_{Ca} (Fig. 10 B, red trace). The overall effect of intracellular acidosis will thus include a stimulation of $I_{Ca,L}$ as a result of intracellular charge screening/binding by H^+ ions, plus inhibition as a result of the H^+-induced rise of $Ca^{2+}{}_i$. Results of mathematically simulating these phenomena (Fig. 10 B, red trace) are in good agreement with the experimental data (Fig. 4 B, left).

The cause of the rise in diastolic Ca^{2+} during intracellular acidosis has not been entirely resolved, but possible mechanisms include displacement of Ca^{2+} from cytoplasmic or mitochondrial buffer sites, H^+-induced slowing of SR Ca^{2+} uptake, and reduced sarcolemmal Ca^{2+} extrusion via NCX (Kohmoto et al., 1990; Orchard and Kentish, 1990; Gambassi et al., 1993). Regardless of mechanism, the Ca^{2+} rise appears to form part of a dual control of $I_{Ca,L}$ by pH_i, which comprises a balance between H^+ stimulation and Ca^{2+} inhibition of the current.

Combined intracellular and extracellular acidosis. Having independently assessed the effects of $H^+{}_i$ and $H^+{}_o$, it is possible to interpret their combined influence on $I_{Ca,L}$. The striking observation here is that a comparable fall of both pH_i and pH_o produces minimal effects on peak $I_{Ca,L}$. The right and leftward shifts in channel gating nearly cancel, so that control and test I-V curves during acidosis are virtually superimposed. This is predicted in the computational model (Fig. 10 C, blue trace), assuming that pH_i and pH_o effects are independent. When BAPTA dialysis is omitted, the experimental result is similar, except that a small $Ca^{2+}{}_i$-dependent inhibition of peak $I_{Ca,L}$ is now evident at positive test voltages, which can again be simulated in the model (Fig. 10 C, red trace, and see cartoon inset). Thus, the inhibitory effect of a fall in pH_o can be offset by a simultaneous fall in pH_i.

CaMKII modulates pH sensitivity? $I_{Ca,L}$ in rat myocytes is reported to be largely insensitive to a combined acidosis, a result attributed to the protective action of intracellular CaMKII activity (Komukai et al., 2001). This cannot be the explanation in the present work, as $I_{Ca,L}$ was similarly modulated by appropriate pH_i displacements before or after enzyme inhibition with KN-93 (Fig. 9). Although our control acid challenges (2 min) may have been too brief for full CaMKII protection to develop, in other experiments (not depicted) we obtained similar results after more prolonged challenges (5–10 min), suggesting that acute anti-acid protection of $I_{Ca,L}$ by CaMKII is not strongly expressed, at least not in rabbit myocytes. Indeed, as discussed above, an appropriate balancing of acute extracellular inhibition with intracellular stimulation, when pH is reduced on both sides of the sarcolemma, can automatically result in an apparent pH insensitivity of $I_{Ca,L}$.

In summary, this work emphasizes that the acute response of peak $I_{Ca,L}$ to acidosis will be highly labile, depending on whether a pH change occurs in the extracellular or intracellular domain, or both, and whether the change is coupled with a significant displacement of diastolic Ca^{2+}.

pH control of $I_{Ca,L}$: Late Ca^{2+} entry

The pH sensitivity of peak $I_{Ca,L}$ is paralleled by a comparable sensitivity of net L-type Ca^{2+} entry during an AP (Fig. 8). Most of this entry occurs during the current's inactivating phase and can therefore be defined as late Ca^{2+} entry, which flows during the AP plateau. Late Ca^{2+} entry is decreased by low pH_o but increased by low pH_i. Results of mathematical modeling (Fig. 11; described below) indicate that the decline in maximal P_{Ca} causes the reduction of late entry during extracellular acidosis, whereas the enhancement of late entry during intracellular acidosis is caused mainly by the H^+-dependent slowing of $I_{Ca,L}$ inactivation. When a combined acidosis is applied, however, the opposing effects of pH_i and pH_o on late Ca^{2+} entry do not cancel as effectively as they do for peak $I_{Ca,L}$. Instead, the slowing of $I_{Ca,L}$ inactivation seen with low pH_i becomes even more pronounced (Fig. 7 C), so that late Ca^{2+} entry is further enhanced. The result emphasizes that pH control of late entry is dominated by changes of pH_i.

The molecular basis of cardiac L-type calcium channel inactivation is unresolved, and various models have been proposed in which VDI and CDI either share a final common pathway (Findlay, 2004; Kim et al., 2004; Findeisen and Minor, 2009) or are mediated independently (Barrett and Tsien, 2008). Although our results do not reveal the site(s) of action of protons on the molecular complexes involved, they demonstrate the opposing effects of H^+ and Ca^{2+} on inactivation kinetics: acidosis slows it, whereas $Ca^{2+}{}_i$ elevation speeds it up.

VDI is thought to make only a small contribution to $I_{Ca,L}$ inactivation over the time course of the ventricular AP (Sun et al., 1997; Linz and Meyer, 1998). Our finding that, when using Na^+ instead of Ca^{2+} as the charge carrier, current inactivation is slowed by low pH_o or pH_i (Fig. S6) suggests that VDI may play a significant role during acidosis.

pH control of the AP

The opposing effects of pH_i and pH_o on late Ca^{2+} entry appear to have major repercussions on the ventricular AP. This work has shown, for the first time, that low pH_o shortens, whereas low pH_i lengthens the AP. Interestingly, combined reduction of pH_o and pH_i lengthens the AP and simultaneously increases late Ca^{2+} entry. As similar changes of late entry were seen with and without intracellular BAPTA (compare Figs. 8 and S7), Ca^{2+}-activated changes of I_{NCX}, which would be buffered out by BAPTA, are unlikely to have significantly affected the estimates of Ca^{2+} entry. Furthermore, in the absence of any pH change, shortening or lengthening the AP (by

using the AP-clamp technique) produced only small effects on net Ca^{2+} entry. It is therefore highly likely that the changes of APD during acidosis are driven primarily by the effects of pH on late Ca^{2+} entry.

A change in AP trajectory can, of course, be caused by H^+-induced modulation of I_{NCX} and K^+ and Cl^- currents (Doering et al., 1996; Xu and Rozanski, 1997; Vereecke and Carmeliet, 2000; Hirayama et al., 2002; Peretz et al., 2002), in addition to effects on $I_{Ca,L}$. Even in the absence of acidosis, a lengthening of the AP and an elevation of its plateau are known to increase late Ca^{2+} entry (Linz and Meyer, 2000; Sah et al., 2003) by slowing Ca^{2+} channel inactivation. The present results, however, indicate that modulation of late Ca^{2+} entry by pH is likely to be the dominant factor controlling APD during an acid–base disturbance. The pH_i versus pH_o sensitivity of the L-type Ca^{2+} channel is thus likely to be a key element controlling myocardial electrical signaling under these conditions.

Modeling pH control of $I_{Ca,L}$, the AP, and Ca^{2+} signaling

To explore the functional effects of pH on Ca^{2+} signaling and the AP, we simulated them using the Shannon et al. (2004) computational model for the rabbit ventricular myocyte, after incorporating the pH sensitivity for $I_{Ca,L}$ and various other Ca^{2+}-handling proteins. The model (represented schematically in Fig. 11 A) comprises flux equations for both channels and transporters, including SR Ca^{2+} release and reuptake. Equations for mitochondrial Ca^{2+} handling and pH regulatory transporters were not included (the latter were inhibited in our experimental work).

Extracellular acidosis. The model predicts a shortening of the AP, which is secondary to the pH_o-induced reduction in late Ca^{2+} entry (Fig. 11 B). Initial peak $I_{Ca,L}$ is also modestly reduced, leading to lower activation of RyRs and a smaller SR Ca^{2+} release. As a result, there is a reduction in the amplitude of the CaT. After 2 min, SR Ca^{2+} content falls, along with a small reduction in diastolic Ca^{2+}. These reductions are predicted to result from the decrease in Ca^{2+} influx via $I_{Ca,L}$, leading to a reduced overall Ca^{2+} content. The decreased Ca^{2+} influx is eventually balanced in the model by a fall in NCX activity, thus producing a decreased Ca^{2+} efflux on the transporter when averaged over the course of a cardiac cycle. In summary, when pH_o effects on $I_{Ca,L}$ are coded into the model, they reproduce the major features of extracellular acidosis: a shorter AP, a reduced $I_{Ca,L}$ and SR Ca^{2+} content, and a reduced CaT amplitude and duration.

Intracellular acidosis. The model predicts AP lengthening, principally because of the enhanced late Ca^{2+} entry, which prolongs $I_{Ca,L}$ during the plateau (Fig. 11 C). The plateau is elevated in low pH_i to more positive values by H^+_i block of I_{to}, the major determinant of the rate of phase 1 repolarization. The elevated plateau, combined with an acid-induced rise in $[Ca^{2+}]_{dia}$, reduces initial peak $I_{Ca,L}$, as observed experimentally during AP clamps (Fig. 8 A). Thus, any direct H^+_i stimulation of peak $I_{Ca,L}$ is offset here by secondary inhibition caused by changes of Ca^{2+}_i and the AP. The predicted amplitude of the CaT is decreased and the recovery phase is slower because of H^+_i-induced reduction in SR Ca^{2+}-ATPare (SERCA) activity. Although both SR Ca^{2+} uptake and release are reduced, SR Ca^{2+} content increases as a result of increased late Ca^{2+} entry via $I_{Ca,L}$. Reduced SERCA activity contributes to the increase in Ca^{2+}_{dia}. Interestingly, the increase of late Ca^{2+} entry is balanced in the steady state by an increase in net Ca^{2+} extrusion via NCX. The computational model thus reproduces the main features of intracellular acidosis: increased late Ca^{2+} entry, a lengthened AP with an elevated plateau, a reduced peak $I_{Ca,L}$, reduced CaT amplitude, and increased SR Ca^{2+} content.

The simulations of extracellular and intracellular acidosis support an important role for the pH sensitivity of $I_{Ca,L}$ in defining electrical and Ca^{2+} signaling activity in the ventricular myocyte. Notable features of the model are: (a) the effect of pH on initial peak $I_{Ca,L}$, which helps to determine the amplitude of the CaT; and (b) the effect on late Ca^{2+} entry, which helps to define the duration of the AP and overall Ca^{2+} influx into the cell. The key to predicting $I_{Ca,L}$ effects in the whole cell is the differential modulation of Ca^{2+} current by pH_i and pH_o, the former being stimulatory and the latter being inhibitory, combined with the influence of acidosis on Ca^{2+}_i. The overall control of $I_{Ca,L}$ by acidosis is summarized schematically in Fig. 12.

Comparison with previous work

Most studies in cardiac myocytes have reported $I_{Ca,L}$ inhibition by acidosis (Kohlhardt et al., 1976; Kurachi, 1982; Yatani and Goto, 1983; Irisawa and Sato, 1986; Kaibara and Kameyama, 1988; Krafte and Kass, 1988; F. Chen et al., 1996; Cheng et al., 2009), although some suggest no effect (Hulme and Orchard, 1998; Komukai et al., 2002; Salameh et al., 2002). It is perhaps surprising that the stimulatory nature of intracellular H^+ ions has not been noted. Several early studies of $I_{Ca,L}$ attempted to manipulate pH_i via pipette dialysis (Kurachi, 1982; Sato et al., 1985; Irisawa and Sato, 1986; Salameh et al., 2002). The pH_i was not monitored, however, and subsequent work showed that accurate pH_i dialysis is very difficult to achieve, given high intracellular H^+ buffering and low H^+_i mobility (Vaughan-Jones et al., 2002). As a result, pH_i may not have been as extensively reduced as assumed, thus obscuring possible stimulatory effects.

An additional problem in some work is likely to have been inadequate inhibition of NHE activity (Kohlhardt et al., 1976; Yatani and Goto, 1983; Krafte and Kass, 1988; Kwan and Kass, 1993; F. Chen et al., 1996;

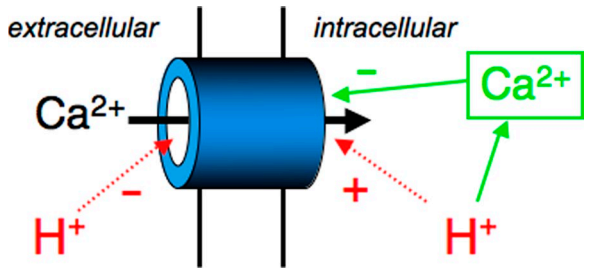

Figure 12. Schematic summary of acidosis effects on $I_{Ca,L}$. Extracellular acidosis decreases peak $I_{Ca,L}$ by directly blocking the channel pore and by shifting current activation toward less negative potentials. It also reduces late Ca^{2+} entry during an AP. In contrast, intracellular acidosis stimulates peak $I_{Ca,L}$ by shifting activation toward more negative potentials. This stimulatory effect is blunted by the H^+-induced rise of diastolic Ca^{2+}, which promotes channel inactivation. Intracellular acidosis also enhances late Ca^{2+} entry during an AP. A mixed response of $I_{Ca,L}$ occurs when pH_i and pH_o changes are imposed simultaneously.

Komukai et al., 2002). As a result, secondary effects on $I_{Ca,L}$ caused by NHE-mediated changes of $Ca^{2+}{}_i$, particularly during intracellular acidosis, may have distorted the data. In some cases, NHE was blocked with amiloride (Irisawa and Sato, 1986), but, unlike cariporide, this drug can directly inhibit $I_{Ca,L}$ (Cheng et al., 2004; present work).

Some reports have examined the effects of combined acidosis on $I_{Ca,L}$ (e.g., Hulme and Orchard, 1998; Komukai et al., 2002). Although important, we now know that such an approach is complex to interpret, given the opposing effects on $I_{Ca,L}$ of pH in intracellular and extracellular domains. In some work, salts of weak acids like acetate and butyrate were used to decrease pH_i, but without compensating for their significant binding of extracellular Ca^{2+} (e.g., ~20% binding by 80 mM acetate or butyrate), which will decrease $I_{Ca,L}$ and acutely reduce CaT amplitude (Choi et al., 2000). To these problems should be added differences in voltage-clamp technique (whole cell vs. perforated patch), working temperature, species, and pH-displacement protocols. Thus, there has been a pressing need to quantify rigorously the effects of pH on $I_{Ca,L}$, Ca^{2+} signaling, and the AP.

Conclusions: Physiological and clinical significance

Intracellular and extracellular pH changes are powerful modulators of $I_{Ca,L}$. Opposing effects can be seen when the two pH domains are separately controlled, with $H^+{}_i$ being stimulatory and $H^+{}_o$ being inhibitory (Fig. 12). A major contributor to these effects appears to be H^+ screening and/or binding to anionic sites on the sarcolemma and Ca^{2+} channel protein, resulting in voltage shifts in gating. Domain effects are expressed within the physiological range ($pK_e \sim pK_i \sim 6.9$; Fig. 5), with maximum and minimum influence exerted over a narrow $[H^+]$ range of 63–316 nM H^+ (pH range of 7.2–6.5). This emphasizes the high potency of H^+ modulation. The present work shows that control of $I_{Ca,L}$ by pH has important implications for myocyte function, producing AP shortening or lengthening, alteration of the CaT, and changes in overall Ca^{2+} loading of the cell. Indeed, the stimulatory effect of intracellular or combined acidosis on late Ca^{2+} entry suggests that the L-type Ca^{2+} channel may be an important contributor to $Ca^{2+}{}_i$ overload under these conditions.

Large pH displacements that occur in clinical situations like myocardial ischemia and reperfusion seriously compromise cardiac contractile and electrical function. When pH displacements occur simultaneously in the extracellular and intracellular domains, acute effects on peak $I_{Ca,L}$ will be minimal, but, as mentioned above, effects on late Ca^{2+} entry may be considerable. When there is disparity between pH changes in the two domains, as may occur during local intracellular metabolic dysfunction, or local fluctuations in extracellular perfusion, a major modulation of both the peak and later phases of $I_{Ca,L}$ is predicted to occur. The present work emphasizes that acute H^+ ion regulation of $I_{Ca,L}$ cannot be ignored when attempting to unravel the physiological and pathophysiological role of pH in the heart.

We gratefully acknowledge helpful discussions with Drs. Pawel Swietach, Michael Sanguinetti, Michael Sheets, Frank Sachse, Derek Terrar, and Francisco Villafuerte, and the technical support of Dr. Philip Ershler. We thank Drs. Juergen Puenter and Heinz-Werner Kleemann of Sanofi-Aventis (Frankford, Germany) for generously providing cariporide and S-0859 for these experiments.

This work was supported by the National Institutes of Health (grant R37HL042873) and the Nora Eccles Treadwell Foundation (to K.W. Spitzer), the Wellcome Trust Human Physiome Project, and British Heart Foundation (to R.D. Vaughan-Jones).

Richard L. Moss served as editor.

Submitted: 28 April 2011
Accepted: 28 September 2011

REFERENCES

Adachi-Akahane, S., L. Cleemann, and M. Morad. 1996. Cross-signaling between L-type Ca^{2+} channels and ryanodine receptors in rat ventricular myocytes. *J. Gen. Physiol.* 108:435–454. http://dx.doi.org/10.1085/jgp.108.5.435

Barrett, C.F., and R.W. Tsien. 2008. The Timothy syndrome mutation differentially affects voltage- and calcium-dependent inactivation of CaV1.2 L-type calcium channels. *Proc. Natl. Acad. Sci. USA.* 105:2157–2162. http://dx.doi.org/10.1073/pnas.0710501105

Bers, D.M. 2001. Excitation-Contraction Coupling and Cardiac Contractile Force. Second edition. Kluwer Academic Publishers, Boston. 427 pp.

Bodi, I., G. Mikala, S.E. Koch, S.A. Akhter, and A. Schwartz. 2005. The L-type calcium channel in the heart: the beat goes on. *J. Clin. Invest.* 115:3306–3317. http://dx.doi.org/10.1172/JCI27167

Bountra, C., K. Kaila, and R.D. Vaughan-Jones. 1988. Effect of repetitive activity upon intracellular pH, sodium and contraction in sheep cardiac Purkinje fibres. *J. Physiol.* 398:341–360.

Bridge, J.H.B., J.R. Smolley, and K.W. Spitzer. 1990. The relationship between charge movements associated with I_{Ca} and $I_{Na\text{-}Ca}$ in cardiac myocytes. *Science.* 248:376–378. http://dx.doi.org/10.1126/science.2158147

Buckler, K.J., and R.D. Vaughan-Jones. 1990. Application of a new pH-sensitive fluoroprobe (carboxy-SNARF-1) for intracellular pH measurement in small, isolated cells. *Pflugers Arch.* 417:234–239. http://dx.doi.org/10.1007/BF00370705

Cens, T., M. Rousset, J.P. Leyris, P. Fesquet, and P. Charnet. 2006. Voltage- and calcium-dependent inactivation in high voltage-gated Ca(2+) channels. *Prog. Biophys. Mol. Biol.* 90:104–117. http://dx.doi.org/10.1016/j.pbiomolbio.2005.05.013

Ch'en, F.F., F.C. Villafuerte, P. Swietach, P.M. Cobden, and R.D. Vaughan-Jones. 2008. S0859, an N-cyanosulphonamide inhibitor of sodium-bicarbonate cotransport in the heart. *Br. J. Pharmacol.* 153:972–982. http://dx.doi.org/10.1038/sj.bjp.0707667

Chen, F., G.T. Wetzel, W.F. Friedman, and T.S. Klitzner. 1996. Developmental changes in the effects of pH on contraction and Ca2+ current in rabbit heart. *J. Mol. Cell. Cardiol.* 28:635–642. http://dx.doi.org/10.1006/jmcc.1996.0059

Chen, X.H., and R.W. Tsien. 1997. Aspartate substitutions establish the concerted action of P-region glutamates in repeats I and III in forming the protonation site of L-type Ca2+ channels. *J. Biol. Chem.* 272:30002–30008. http://dx.doi.org/10.1074/jbc.272.48.30002

Chen, X.H., I. Bezprozvanny, and R.W. Tsien. 1996. Molecular basis of proton block of L-type Ca^{2+} channels. *J. Gen. Physiol.* 108:363–374. http://dx.doi.org/10.1085/jgp.108.5.363

Cheng, H., G.L. Smith, C.H. Orchard, and J.C. Hancox. 2009. Acidosis inhibits spontaneous activity and membrane currents in myocytes isolated from the rabbit atrioventricular node. *J. Mol. Cell. Cardiol.* 46:75–85. http://dx.doi.org/10.1016/j.yjmcc.2008.09.709

Cheng, L., F. Wang, H.Y. Zhou, W.X. Yao, G.J. Xia, and M.X. Jiang. 2004. Effects of amiloride on potassium and calcium currents in guinea pig ventricular myocytes. *Yao Xue Xue Bao.* 39:509–513.

Choi, H.S., A.W. Trafford, C.H. Orchard, and D.A. Eisner. 2000. The effect of acidosis on systolic Ca2+ and sarcoplasmic reticulum calcium content in isolated rat ventricular myocytes. *J. Physiol.* 529:661–668. http://dx.doi.org/10.1111/j.1469-7793.2000.00661.x

DeSantiago, J., L.S. Maier, and D.M. Bers. 2004. Phospholamban is required for CaMKII-dependent recovery of Ca transients and SR Ca reuptake during acidosis in cardiac myocytes. *J. Mol. Cell. Cardiol.* 36:67–74. http://dx.doi.org/10.1016/j.yjmcc.2003.10.012

Doering, A.E., D.A. Eisner, and W.J. Lederer. 1996. Cardiac Na-Ca exchange and pH. *Ann. NY Acad. Sci.* 779:182–198. http://dx.doi.org/10.1111/j.1749-6632.1996.tb44786.x

Dolphin, A.C. 2006. A short history of voltage-gated calcium channels. *Br. J. Pharmacol.* 147:S56–S62. http://dx.doi.org/10.1038/sj.bjp.0706442

Egger, M., and E. Niggli. 2000. Paradoxical block of the Na^{+}-Ca^{2+} exchanger by extracellular protons in guinea-pig ventricular myocytes. *J. Physiol.* 523:353–366. http://dx.doi.org/10.1111/j.1469-7793.2000.t01-1-00353.x

Elliott, A.C., G.L. Smith, and D.G. Allen. 1994. The metabolic consequences of an increase in the frequency of stimulation in isolated ferret hearts. *J. Physiol.* 474:147–159.

Ferreira, G., J. Yi, E. Ríos, and R. Shirokov. 1997. Ion-dependent inactivation of barium current through L-type calcium channels. *J. Gen. Physiol.* 109:449–461. http://dx.doi.org/10.1085/jgp.109.4.449

Findeisen, F., and D.L. Minor Jr. 2009. Disruption of the IS6-AID linker affects voltage-gated calcium channel inactivation and facilitation. *J. Gen. Physiol.* 133:327–343. http://dx.doi.org/10.1085/jgp.200810143

Findlay, I. 2004. Physiological modulation of inactivation in L-type Ca2+ channels: one switch. *J. Physiol.* 554:275–283. http://dx.doi.org/10.1113/jphysiol.2003.047902

Frankenhaeuser, B., and A.L. Hodgkin. 1957. The action of calcium on the electrical properties of squid axons. *J. Physiol.* 137:218–244.

Gambassi, G., R.G. Hansford, S.J. Sollott, B.A. Hogue, E.G. Lakatta, and M.C. Capogrossi. 1993. Effects of acidosis on resting cytosolic and mitochondrial Ca^{2+} in mammalian myocardium. *J. Gen. Physiol.* 102:575–597. http://dx.doi.org/10.1085/jgp.102.3.575

Gao, L., L.A. Blair, and J. Marshall. 2006. CaMKII-independent effects of KN93 and its inactive analog KN92: reversible inhibition of L-type calcium channels. *Biochem. Biophys. Res. Commun.* 345:1606–1610. http://dx.doi.org/10.1016/j.bbrc.2006.05.066

Garlick, P.B., G.K. Radda, and P.J. Seeley. 1979. Studies of acidosis in the ischaemic heart by phosphorus nuclear magnetic resonance. *Biochem. J.* 184:547–554.

Hacht, B. 2008. Complex formation of acetic acid with Ca(II) and Mg(II) under physiological conditions. *J. Solution Chem.* 37:155–163. http://dx.doi.org/10.1007/s10953-007-9233-3

Hanck, D.A., and M.F. Sheets. 1992. Extracellular divalent and trivalent cation effects on sodium current kinetics in single canine cardiac Purkinje cells. *J. Physiol.* 454:267–298.

Hille, B. 2001. Ion Channels of Excitable Membranes. Third edition. Sinauer Associates, Inc., Sunderland, MA. 814 pp.

Hirayama, Y., A. Kuruma, M. Hiraoka, and S. Kawano. 2002. Calcium-activated CL− current is enhanced by acidosis and contributes to the shortening of action potential duration in rabbit ventricular myocytes. *Jpn. J. Physiol.* 52:293–300. http://dx.doi.org/10.2170/jjphysiol.52.293

Höfer, G.F., K. Hohenthanner, W. Baumgartner, K. Groschner, N. Klugbauer, F. Hofmann, and C. Romanin. 1997. Intracellular Ca2+ inactivates L-type Ca2+ channels with a Hill coefficient of approximately 1 and an inhibition constant of approximately 4 microM by reducing channel's open probability. *Biophys. J.* 73:1857–1865. http://dx.doi.org/10.1016/S0006-3495(97)78216-X

Hulme, J.T., and C.H. Orchard. 1998. Effect of acidosis on Ca2+ uptake and release by sarcoplasmic reticulum of intact rat ventricular myocytes. *Am. J. Physiol.* 275:H977–H987.

Irisawa, H., and R. Sato. 1986. Intra- and extracellular actions of proton on the calcium current of isolated guinea pig ventricular cells. *Circ. Res.* 59:348–355.

Isenberg, G., and U. Klöckner. 1982. Calcium currents of isolated bovine ventricular myocytes are fast and of large amplitude. *Pflugers Arch.* 395:30–41. http://dx.doi.org/10.1007/BF00584965

Josephson, I.R., J. Sanchez-Chapula, and A.M. Brown. 1984. A comparison of calcium currents in rat and guinea pig single ventricular cells. *Circ. Res.* 54:144–156.

Josephson, I.R., A. Guia, E.G. Lakatta, W.J. Lederer, and M.D. Stern. 2010. Ca(2+)-dependent components of inactivation of unitary cardiac L-type Ca(2+) channels. *J. Physiol.* 588:213–223. http://dx.doi.org/10.1113/jphysiol.2009.178343

Kaibara, M., and M. Kameyama. 1988. Inhibition of the calcium channel by intracellular protons in single ventricular myocytes of the guinea-pig. *J. Physiol.* 403:621–640.

Kenyon, J.L., and W.R. Gibbons. 1977. Effects of low-chloride solutions on action potentials of sheep cardiac Purkinje fibers. *J. Gen. Physiol.* 70:635–660.

Kass, R.S., and M.C. Sanguinetti. 1984. Inactivation of calcium channel current in the calf cardiac Purkinje fiber. Evidence for voltage- and calcium-mediated mechanisms. *J. Gen. Physiol.* 84:705–726. http://dx.doi.org/10.1085/jgp.84.5.705

Kentish, J.C., and J.Z. Xiang. 1997. Ca^{2+}- and caffeine-induced Ca^{2+} release from the sarcoplasmic reticulum in rat skinned trabeculae: effects of pH and P_i. *Cardiovasc. Res.* 33:314–323. http://dx.doi.org/10.1016/S0008-6363(96)00217-9

Kim, J., S. Ghosh, D.A. Nunziato, and G.S. Pitt. 2004. Identification of the components controlling inactivation of voltage-gated Ca2+ channels. *Neuron.* 41:745–754. http://dx.doi.org/10.1016/S0896-6273(04)00081-9

Kohlhardt, M., K. Haap, and H.R. Figulla. 1976. Influence of low extracellular pH upon the Ca inward current and isometric contractile force in mammalian ventricular myocardium. *Pflugers Arch.* 366:31–38. http://dx.doi.org/10.1007/BF02486557

Kohmoto, O., K.W. Spitzer, M.A. Movsesian, and W.H. Barry. 1990. Effects of intracellular acidosis on [Ca2+]i transients, transsarcolemmal Ca2+ fluxes, and contraction in ventricular myocytes. *Circ. Res.* 66:622–632.

Kokubun, S., and H. Irisawa. 1984. Effects of various intracellular Ca ion concentrations on the calcium current of guinea-pig single ventricular cells. *Jpn. J. Physiol.* 34:599–611. http://dx.doi.org/10.2170/jjphysiol.34.599

Komukai, K., C. Pascarel, and C.H. Orchard. 2001. Compensatory role of CaMKII on ICa and SR function during acidosis in rat ventricular myocytes. *Pflugers Arch.* 442:353–361. http://dx.doi.org/10.1007/s004240100549

Komukai, K., F. Brette, C. Pascarel, and C.H. Orchard. 2002. Electrophysiological response of rat ventricular myocytes to acidosis. *Am. J. Physiol. Heart Circ. Physiol.* 283:H412–H422.

Krafte, D.S., and R.S. Kass. 1988. Hydrogen ion modulation of Ca channel current in cardiac ventricular cells. Evidence for multiple mechanisms. *J. Gen. Physiol.* 91:641–657. http://dx.doi.org/10.1085/jgp.91.5.641

Kurachi, Y. 1982. The effects of intracellular protons on the electrical activity of single ventricular cells. *Pflugers Arch.* 394:264–270. http://dx.doi.org/10.1007/BF00589102

Kwan, Y.W., and R.S. Kass. 1993. Interactions between H+ and Ca2+ near cardiac L-type calcium channels: evidence for independent channel-associated binding sites. *Biophys. J.* 65:1188–1195. http://dx.doi.org/10.1016/S0006-3495(93)81152-4

Lacinová, L., and F. Hofmann. 2005. Ca2+- and voltage-dependent inactivation of the expressed L-type Ca(v)1.2 calcium channel. *Arch. Biochem. Biophys.* 437:42–50. http://dx.doi.org/10.1016/j.abb.2005.02.025

Lee, K.S., E. Marban, and R.W. Tsien. 1985. Inactivation of calcium channels in mammalian heart cells: joint dependence on membrane potential and intracellular calcium. *J. Physiol.* 364:395–411.

Linz, K.W., and R. Meyer. 1998. Control of L-type calcium current during the action potential of guinea-pig ventricular myocytes. *J. Physiol.* 513:425–442. http://dx.doi.org/10.1111/j.1469-7793.1998.425bb.x

Linz, K.W., and R. Meyer. 2000. Profile and kinetics of L-type calcium current during the cardiac ventricular action potential compared in guinea-pigs, rats and rabbits. *Pflugers Arch.* 439:588–599. http://dx.doi.org/10.1007/s004240050982

Luo, C.H., and Y. Rudy. 1994. A dynamic model of the cardiac ventricular action potential. I. Simulations of ionic currents and concentration changes. *Circ. Res.* 74:1071–1096.

Mahajan, A., Y. Shiferaw, D. Sato, A. Baher, R. Olcese, L.H. Xie, M.J. Yang, P.S. Chen, J.G. Restrepo, A. Karma, et al. 2008. A rabbit ventricular action potential model replicating cardiac dynamics at rapid heart rates. *Biophys. J.* 94:392–410. http://dx.doi.org/10.1529/biophysj.106.98160

Matsuda, H. 1986. Sodium conductance in calcium channels of guinea-pig ventricular cells induced by removal of external calcium ions. *Pflugers Arch.* 407:465–475. http://dx.doi.org/10.1007/BF00657502

Mattiazzi, A., L. Vittone, and C. Mundiña-Weilenmann. 2007. Ca2+/calmodulin-dependent protein kinase: a key component in the contractile recovery from acidosis. *Cardiovasc. Res.* 73:648–656. http://dx.doi.org/10.1016/j.cardiores.2006.12.002

Nakajima, I., H. Watanabe, K. Iino, T. Saito, and M. Miura. 2002. Ca2+ overload evokes a transient outward current in guinea-pig ventricular myocytes. *Circ. J.* 66:87–92. http://dx.doi.org/10.1253/circj.66.87

Nomura, N., H. Satoh, H. Terada, M. Matsunaga, H. Watanabe, and H. Hayashi. 2002. CaMKII-dependent reactivation of SR Ca(2+) uptake and contractile recovery during intracellular acidosis. *Am. J. Physiol. Heart Circ. Physiol.* 283:H193–H203.

Orchard, C.H., and J.C. Kentish. 1990. Effects of changes of pH on the contractile function of cardiac muscle. *Am. J. Physiol.* 258:C967–C981.

Peretz, A., H. Schottelndreier, L.B. Aharon-Shamgar, and B. Attali. 2002. Modulation of homomeric and heteromeric KCNQ1 channels by external acidification. *J. Physiol.* 545:751–766. http://dx.doi.org/10.1113/jphysiol.2002.028381

Post, J.A., G.A. Langer, J.A.F. Op den Kamp, and A.J. Verkleij. 1988. Phospholipid asymmetry in cardiac sarcolemma. Analysis of intact cells and 'gas-dissected' membranes. *Biochim. Biophys. Acta.* 943:256–266. http://dx.doi.org/10.1016/0005-2736(88)90557-3

Sabirov, R.Z., Y. Okada, and S. Oiki. 1997. Two-sided action of protons on an inward rectifier K+ channel (IRK1). *Pflugers Arch.* 433:428–434. http://dx.doi.org/10.1007/s004240050296

Sah, R., R.J. Ramirez, G.Y. Oudit, D. Gidrewicz, M.G. Trivieri, C. Zobel, and P.H. Backx. 2003. Regulation of cardiac excitation-contraction coupling by action potential repolarization: role of the transient outward potassium current (I_{to}). *J. Physiol.* 546:5–18. http://dx.doi.org/10.1113/jphysiol.2002.026468

Salameh, A., S. Dhein, and D.J. Beuckelmann. 2002. Role of the cardiac Na(+)/H(+)exchanger in [Ca(2+)](i) and [Na(+)](i) handling during intracellular acidosis. Effect of cariporide (Hoe 642). *Pharmacol. Res.* 45:35–41. http://dx.doi.org/10.1006/phrs.2001.0908

Sato, R., A. Noma, Y. Kurachi, and H. Irisawa. 1985. Effects of intracellular acidification on membrane currents in ventricular cells of the guinea pig. *Circ. Res.* 57:553–561.

Sham, J.S. 1997. Ca2+ release-induced inactivation of Ca2+ current in rat ventricular myocytes: evidence for local Ca2+ signalling. *J. Physiol.* 500:285–295.

Shannon, T.R., K.S. Ginsburg, and D.M. Bers. 2000. Potentiation of fractional sarcoplasmic reticulum calcium release by total and free intra-sarcoplasmic reticulum calcium concentration. *Biophys. J.* 78:334–343. http://dx.doi.org/10.1016/S0006-3495(00)76596-9

Shannon, T.R., F. Wang, J. Puglisi, C. Weber, and D.M. Bers. 2004. A mathematical treatment of integrated Ca dynamics within the ventricular myocyte. *Biophys. J.* 87:3351–3371. http://dx.doi.org/10.1529/biophysj.104.047449

Sipido, K.R., E. Carmeliet, and F. Van de Werf. 1998. T-type Ca2+ current as a trigger for Ca2+ release from the sarcoplasmic reticulum in guinea-pig ventricular myocytes. *J. Physiol.* 508:439–451. http://dx.doi.org/10.1111/j.1469-7793.1998.439bq.x

Spitzer, K.W., and J.H. Bridge. 1992. Relationship between intracellular pH and tension development in resting ventricular muscle and myocytes. *Am. J. Physiol.* 262:C316–C327.

Sun, H., N. Leblanc, and S. Nattel. 1997. Mechanisms of inactivation of L-type calcium channels in human atrial myocytes. *Am. J. Physiol.* 272:H1625–H1635.

Thomas, R.C. 1984. Experimental displacement of intracellular pH and the mechanism of its subsequent recovery. *J. Physiol.* 354:3P–22P.

Tseng, G.N., and P.A. Boyden. 1991. Different effects of intracellular Ca and protein kinase C on cardiac T and L Ca currents. *Am. J. Physiol.* 261:H364–H379.

Tsien, R.Y. 1980. New calcium indicators and buffers with high selectivity against magnesium and protons: design, synthesis, and properties of prototype structures. *Biochemistry.* 19:2396–2404. http://dx.doi.org/10.1021/bi00552a018

Vaughan-Jones, R.D., B.E. Peercy, J.P. Keener, and K.W. Spitzer. 2002. Intrinsic H(+) ion mobility in the rabbit ventricular myocyte. *J. Physiol.* 541:139–158. http://dx.doi.org/10.1113/jphysiol.2001.013267

Vaughan-Jones, R.D., K.W. Spitzer, and P. Swietach. 2009. Intracellular pH regulation in heart. *J. Mol. Cell. Cardiol.* 46:318–331. http://dx.doi.org/10.1016/j.yjmcc.2008.10.024

Vereecke, J., and E. Carmeliet. 2000. The effect of external pH on the delayed rectifying K+ current in cardiac ventricular myocytes. *Pflugers Arch.* 439:739–751. http://dx.doi.org/10.1007/s004240051000

Wu, Y., L.B. MacMillan, R.B. McNeill, R.J. Colbran, and M.E. Anderson. 1999. CaM kinase augments cardiac L-type Ca2+ current: a cellular mechanism for long Q-T arrhythmias. *Am. J. Physiol.* 276:H2168–H2178.

Xu, L., G. Mann, and G. Meissner. 1996. Regulation of cardiac Ca2+ release channel (ryanodine receptor) by Ca2+, H+, Mg2+, and adenine nucleotides under normal and simulated ischemic conditions. *Circ. Res.* 79:1100–1109.

Xu, Z., and G.J. Rozanski. 1997. Proton inhibition of transient outward potassium current in rat ventricular myocytes. *J. Mol. Cell. Cardiol.* 29:481–490.

Yamamoto, T., P. Swietach, A. Rossini, S.H. Loh, R.D. Vaughan-Jones, and K.W. Spitzer. 2005. Functional diversity of electrogenic Na+-HCO3- cotransport in ventricular myocytes from rat, rabbit and guinea pig. *J. Physiol.* 562:455–475. http://dx.doi.org/10.1113/jphysiol.2004.071068

Yan, G.X., and A.G. Kléber. 1992. Changes in extracellular and intracellular pH in ischemic rabbit papillary muscle. *Circ. Res.* 71:460–470.

Yatani, A., and M. Goto. 1983. The effect of extracellular low pH on the plateau current in isolated, single rat ventricular cells—a voltage clamp study. *Jpn. J. Physiol.* 33:403–415. http://dx.doi.org/10.2170/jjphysiol.33.403

You, Y., D.J. Pelzer, and S. Pelzer. 1995. Trypsin and forskolin decrease the sensitivity of L-type calcium current to inhibition by cytoplasmic free calcium in guinea pig heart muscle cells. *Biophys. J.* 69:1838–1846. http://dx.doi.org/10.1016/S0006-3495(95)80054-8

You, Y., D.J. Pelzer, and S. Pelzer. 1997. Modulation of L-type Ca2+ current by fast and slow Ca2+ buffering in guinea pig ventricular cardiomyocytes. *Biophys. J.* 72:175–187. http://dx.doi.org/10.1016/S0006-3495(97)78656-9

Yuan, W., K.S. Ginsburg, and D.M. Bers. 1996. Comparison of sarcolemmal calcium channel current in rabbit and rat ventricular myocytes. *J. Physiol.* 493:733–746.

Yue, D.T., P.H. Backx, and J.P. Imredy. 1990. Calcium-sensitive inactivation in the gating of single calcium channels. *Science.* 250:1735–1738. http://dx.doi.org/10.1126/science.2176745